Review Article

Targeted magnetic resonance imaging (tMRI) of small changes in the T_1 and spatial properties of normal or near normal appearing white and gray matter in disease of the brain using divided subtracted inversion recovery (dSIR) and divided reverse subtracted inversion recovery (drSIR) sequences

Ya-Jun Ma[1], Dina Moazamian[1], John D. Port[2], Myriam Edjlali[3,4], Jean-Pierre Pruvo[5,6,7], Lotfi Hacein-Bey[8], Nigel Hoggard[9], Martyn N. J. Paley[9], David K. Menon[10], David Bonekamp[11], Emanuele Pravatà[12,13], Michael Garwood[14,15], Helen Danesh-Meyer[16,17,18,19], Paul Condron[18,19], Daniel M. Cornfeld[18,19], Samantha J. Holdsworth[18,19], Jiang Du[1,20,21], Graeme M. Bydder[1,18]

[1]Department of Radiology, University of California San Diego, San Diego, CA, USA; [2]Department of Radiology, Mayo Clinic, Rochester, MN, USA; [3]Department of Radiology, APHP, Hôpitaux Raymond-Poincaré, Paris, France; [4]Laboratoire d'Imagerie Biomédicale Multimodale (BioMaps), Université Paris-Saclay, CEA, CNRS, Inserm, Service Hospitalier Frédéric Joliot, Orsay, France; [5]Inserm, U1172-LilNCog-Lille Neuroscience & Cognition, Univ Lille, Lille, France; [6]UMS 2014-US 41-PLBS-Plateformes Lilloises en Biologie & Santé, Univ Lille, Lille, France; [7]Department of Neuroradiology, CHU Lille, Rue Emile Laine, Lille, France; [8]Neuroradiology, Radiology Department, University of California Davis School of Medicine, Sacramento, CA, USA; [9]Academic Unit of Radiology, Department of Infection, Immunity and Cardiovascular Disease, The Medical School, University of Sheffield, Sheffield, UK; [10]Division of Anaesthesia, University of Cambridge, Addenbrooke's Hospital, Cambridge, UK; [11]Division of Radiology (E010), German Cancer Research Center (DKFZ), Heidelberg, Germany; [12]Department of Neuroradiology, Neurocenter of Southern Switzerland, Lugano, Switzerland; [13]Faculty of Biomedical Sciences, Universita della Svizzera Italiana, Lugano, Switzerland; [14]Center for Magnetic Resonance Research and Department of Radiology, University of Minnesota, Minneapolis, MN, USA; [15]Department of Biomedical Engineering, University of Minnesota, Minneapolis, MN, USA; [16]Department of Ophthalmology, University of Auckland, Auckland, New Zealand; [17]Eye Institute, Auckland, New Zealand; [18]Mātai Medical Research Institute, Tairāwhiti Gisborne, New Zealand; [19]Department of Anatomy and Medical Imaging and Centre for Brain Research, Faculty of Medical and Health Sciences, University of Auckland, Auckland, New Zealand; [20]Research Service, Veterans Affairs San Diego Healthcare System, San Diego, CA, USA; [21]Department of Bioengineering, University of California San Diego, San Diego, CA, USA

Contributions: (I) Conception and design: All authors; (II) Administrative support: YJ Ma, SJ Holdsworth, J Du; (III) Provision of study materials or patients: YJ Ma, D Moazamian, DM Cornfeld, P Condron, SJ Holdsworth; (IV) Collection and assembly of data: YJ Ma, D Moazamian, DM Cornfeld, P Condron; (V) Data analysis and interpretation: YJ Ma, D Moazamian, DM Cornfeld, P Condron; (VI) Manuscript writing: All authors; (VII) Final approval of manuscript: All authors.

Correspondence to: Graeme M. Bydder, MB, ChB. Department of Radiology, University of California San Diego, 9452 Medical Center Drive, San Diego, CA 92037, USA; Mātai Medical Research Institute, Tairāwhiti Gisborne, New Zealand. Email: gbydder@health.ucsd.edu.

Abstract: This review describes targeted magnetic resonance imaging (tMRI) of small changes in the T_1 and the spatial properties of normal or near normal appearing white or gray matter in disease of the brain. It employs divided subtracted inversion recovery (dSIR) and divided reverse subtracted inversion recovery (drSIR) sequences to increase the contrast produced by small changes in T_1 by up to 15 times compared to conventional T_1-weighted inversion recovery (IR) sequences such as magnetization prepared-rapid acquisition gradient echo (MP-RAGE). This increase in contrast can be used to reveal disease with only small changes in T_1 in normal appearing white or gray matter that is not apparent on conventional MP-RAGE, T_2-weighted spin echo (T_2-wSE) and/or fluid attenuated inversion recovery (T_2-FLAIR) images. The small changes in T_1 or T_2 in disease are insufficient to produce useful contrast with conventional sequences. To produce high contrast

dSIR and drSIR sequences typically need to be targeted for the nulling TI of normal white or gray matter, as well as for the sign and size of the change in T_1 in these tissues in disease. The dSIR sequence also shows high signal boundaries between white and gray matter. dSIR and drSIR are essentially T_1 maps. There is a nearly linear relationship between signal and T_1 in the middle domain (mD) of the two sequences which includes T_1s between the nulling T_1s of the two acquired IR sequences. The drSIR sequence is also very sensitive to reductions in T_1 produced by Gadolinium based contrast agents (GBCAs), and when used with rigid body registration to align three-dimensional (3D) isotropic pre and post GBCA images may be of considerable value in showing subtle GBCA enhancement. In serial MRI studies performed at different times, the high signal boundaries generated by dSIR and drSIR sequences can be used with rigid body registration of 3D isotropic images to demonstrate contrast arising from small changes in T_1 (without or with GBCA enhancement) as well as small changes in the spatial properties of normal tissues and lesions, such as their site, shape, size and surface. Applications of the sequences in cases of multiple sclerosis (MS) and methamphetamine dependency are illustrated. Using targeted narrow mD dSIR sequences, widespread abnormalities were seen in areas of normal appearing white matter shown with conventional T_2-wSE and T_2-FLAIR sequences. Understanding of the features of dSIR and drSIR images is facilitated by the use of their T_1-bipolar filters; to explain their targeting, signal, contrast, boundaries, T_1 mapping and GBCA enhancement. Targeted MRI (tMRI) using dSIR and drSIR sequences may substantially improve clinical MRI of the brain by providing unequivocal demonstration of abnormalities that are not seen with conventional sequences.

Keywords: Magnetic resonance imaging (MRI); targeted MRI (tMRI); divided subtracted inversion recovery (dSIR); divided reverse subtracted inversion recovery (drSIR); T_1-bipolar filters; multiple sclerosis (MS); neuroinflammation

Submitted Feb 26, 2023. Accepted for publication Jul 11, 2023. Published online Aug 15, 2023.
doi: 10.21037/qims-23-232
View this article at: https://dx.doi.org/10.21037/qims-23-232

Introduction

In the first study of multiple sclerosis (MS) with magnetic resonance imaging (MRI) in 1981, an intermediate inversion time (TI) T_1-weighted inversion recovery (IR) pulse sequence was used to produce high contrast visualization of lesions with increased T_1s (1). This was followed by the use of long repetition time (TR), long echo time (TE) T_2-weighted spin echo (T_2-wSE) sequences in 1982 and 1983 to show lesions in MS and other diseases with high contrast as a result of their increased T_2s (2-5).

In 1984, a Gadolinium based contrast agent (GBCA) was used with intermediate TI (TI_i) T_1-weighted IR sequences to provide high contrast in lesions as a result of the reduction in T_1 produced by the GBCA (6).

In 1985, the short TI IR (STIR) sequence was described (7). For concurrent increases in T_1 and T_2 in lesions in disease, this sequence displayed synergistic contrast in which the contributions to lesion contrast from both the increases in T_1 and T_2 were complementary. This resulted in high contrast visualization of abnormalities in diseases of the brain and body.

In the same paper (7), the double IR (DIR) sequence was described in which two IR sequences with different TIs were multiplied together. The DIR sequence was used to simultaneously suppress signal from fat and cerebrospinal fluid (CSF). In addition, as with the STIR sequence, concurrent increases in the T_1 and T_2 of lesions produced high synergistic contrast. In 1994, the DIR sequence was used to suppress signal from white or gray matter in the brain, as well as CSF. In lesions with concurrent increases in T_1 and T_2, the sequence provides synergistic T_1 and T_2 contrast in gray or white matter respectively (8).

The T_2-fluid attenuated inversion recovery (T_2-FLAIR) sequence was described in 1992. It used a long TI (TI_l) to suppress CSF signal and a long TE to increase T_2 contrast since, for concurrent increases in T_1 and T_2 in lesions, the T_1 contrast is opposed to the T_2 contrast. The increased T_2-weighting provided by the long TE is used to overcome this, and render the sequence T_2-weighted for most lesions (9).

IR sequences including TI_i IR sequences such as

magnetization prepared-rapid acquisition gradient echo (MP-RAGE), GBCA enhanced TI_i IR acquisitions, STIR and T_2-FLAIR are key components of present day MRI protocols for the study of MS in the brain and spinal cord (10) as well as for tumors (11) and other diseases of the brain (12).

In 2010, in addition to the DIR sequence, another multiplied IR (MIR) sequence, magnetization prepared 2 rapid acquisition gradient echo (MP2RAGE), was described (13) and this has been used to visualize MS lesions in the brain and spinal cord with performance superior to conventional sequences (14,15). The MP2RAGE sequence uses changes in T_1 twice to generate synergistic T_1 contrast from two IR images with different TIs. The images are multiplied together, and the product is normalized by dividing it by the sum of the squares of the signals from both IR images. The sequence contrast is optimized for composite white-gray matter, white matter-CSF, and gray matter-CSF contrasts and uses two widely separated fixed TIs. This provides sensitivity to differences in T_1 in normal and abnormal tissue over a wide domain of T_1 values.

Subtracted IR (SIR) sequences with different TI_s were described in 2017 and 2018 (16,17). The SIR sequence provides images with increased T_1 dependent contrast compared with single IR sequences for T_1s between the nulling values for the two TIs of the IR sequences. The TIs of the two IR sequences were narrowly separated and were varied depending on the tissue(s) of interest.

Variants of the fluid and white matter suppression (FLAWS) sequence in which two IR images with different TIs are subtracted, and then divided by the sum of the two images were described in 2019 and 2021 (18,19). These FLAWS high contrast (FLAWS-hc) and FLAWS-hc opposite (FLAWS-hco) sequences use two widely separate fixed TIs and provided T_1 contrast over a wide domain of T_1 values.

In four previous papers published in 2020 and 2022, a formalism was described to understand the signal, contrast and weighting of MRI pulse sequences using the concepts of tissue property filters (TP-filters) and the central contrast theorem (CCT) (20-23). This approach uses a quantitative definition of sequence weighting to understand the contrast produced by commonly used clinical sequences as well as more complex sequences. Combinations of two or more IR sequences were generalized as the multiplication, addition, subtraction, and/or division of IR (MASDIR) group of sequences. Contrast in these sequences was mathematically modeled using TP-filters and the CCT.

In modeling contrast produced by MASDIR sequences, two particularly interesting sequences were identified. These were forms of the divided SIR (dSIR) sequence in which two magnitude IR images with different TIs were subtracted and divided by the sum of the two images, and a variant of this, the divided reverse SIR (drSIR) sequence, in which the subtraction of the two IR images is performed in the reverse order. Both sequences employ differences or changes in T_1 on 3–4 occasions to generate synergistic T_1 contrast. The middle domain (mD) of the dSIR and drSIR sequences includes T_1s between the nulled T_1s of the original two IR sequences. When narrow mD versions of the dSIR and drSIR sequences were used, small changes in T_1 produced 5–15 times the contrast seen with conventional MP-RAGE sequences. This was particularly well suited to demonstrating contrast due to small changes in T_1 in normal or near normal appearing white matter (as shown with conventional T_2-wSE and T_2-FLAIR sequences). Using narrow mD dSIR sequences in cases of MS, extensive abnormalities were demonstrated in areas of normal appearing white matter [e.g., *Fig. 31-35* in (23)].

Narrow mD dSIR and drSIR sequences are very sensitive to small changes in T_1 within the narrow mD. This differs from MP2RAGE, FLAWS-hc, and FLAWS-hco sequences which are generally less sensitive to small changes in T_1 than narrow mD dSIR and drSIR sequences in the mD, but are sensitive to changes in T_1 over a wider domain of T_1 values.

The term targeted MRI (tMRI) is used to describe sequences which are focused on a particular tissue and specific changes in one or more tissue properties (TPs) of that tissue such as T_1 and T_2. In this paper, the dSIR and drSIR sequences are targeted at small changes in T_1 from normal in normal or near normal appearing white or gray matter. This requires use of TIs targeted at the nulling TIs of normal white and gray matter as well as different TIs to match the sign and size of changes in T_1 expected in disease. This is different to MP2RAGE, FLAWS-hc, and FLAWS-hco sequences which use fixed TIs for all tissues and are not targeted at a specific tissue or specific changes in the T_1 of that tissue in disease.

In addition to the production of high contrast from small changes in tissue T_1 using narrow mDs described above, dSIR and drSIR sequences can produce high signal, often high contrast boundaries between tissues and fluids. (The term "tissues" is used to include tissues and fluids in the rest of this paper unless otherwise specified.)

dSIR and drSIR images are normalized, and are largely independent of mobile proton density (ρ_m) and T_2 (which both cancel out in the dSIR and drSIR signal equations),

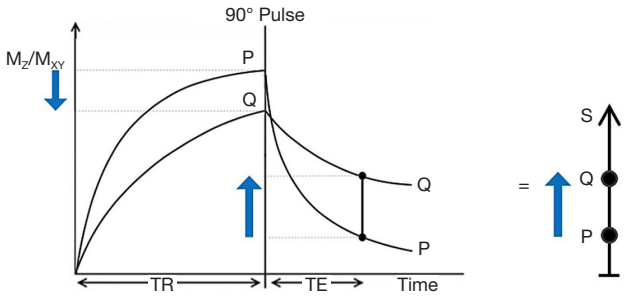

Figure 1 Plot of M_Z/M_{XY} *vs.* time for the SE sequence for two tissues P (with a shorter T_1 and T_2) and Q (with a longer T_1 and T_2). T_1-dependent contrast (first negative blue arrow on left), and overall T_1 and T_2 contrast (second = third positive blue arrows in center and on right) are shown. TR, repetition time; TE, echo time; SE, spin echo.

and are therefore essentially T_1 maps. In the mD, image signal is, to a first approximation, proportional to T_1.

The drSIR sequence is very sensitive to small reductions in T_1 produced by GBCAs and the sequence can be used with three-dimensional (3D) isotropic acquisitions and rigid body registration to eliminate misregistration between pre- and post-GBCA images, and show GBCA enhancement in normal and diseased tissue.

The high signal boundaries of dSIR and drSIR sequences can be used with rigid body registration to show small changes in spatial properties (e.g., site, shape, size and surface) of normal anatomical structures and lesions over time in serial studies. This is in addition to changes in T_1.

The availability of T_1 measurements and sharply defined boundaries with dSIR and drSIR sequences makes them well suited to quantification of T_1 without or with GBCA enhancement, as well as the spatial properties of normal tissues and lesions.

The purpose of this article is to explain the background underpinning the use of dSIR and drSIR sequences to target small changes in the T_1 and spatial properties of normal (or near normal) white matter or gray matter of the brain, describe implementation of the sequences and illustrate their use in clinical cases.

Theory

The spin echo (SE) sequence (univariate model)

The usual explanation of image signal and contrast with the SE sequence utilizes a simplified version of the Bloch equations. This initially follows longitudinal magnetization (M_Z) over time TR and, after the application of a 90° pulse, then follows transverse magnetization (M_{XY}) over time TE (*Figure 1*). Contrast between two tissues such as P with a shorter T_1 and T_2, and Q with a longer T_1 and T_2, is shown by the vertical difference in M_{XY} at the time of data collection TE, as shown by the vertical blue arrow on the right in *Figure 1*. M_Z becomes M_{XY} as a result of the 90° pulse used in the SE sequence.

The voxel signal S for a SE sequence is derived from the simplified Bloch equations where:

$$S = K\rho_m\left(1-e^{-t'/T_1}\right)e^{-t''/T_2} \quad [1]$$

K is a scaling function, ρ_m is mobile proton density, t' is the variable time for the initial part of the sequence, and t" is the variable time for the latter part of the sequence. T_1 and T_2 are time constants. Eq. [1] describes ρ_m in the first segment, recovery of longitudinal magnetization (M_Z) over time in the second segment (which is in parentheses), and decay of transverse magnetization (M_{XY}) over time in the third segment. The equations in the second and third segments are of the forms $y = 1 - e^{-x}$ and $y = e^{-x}$, respectively where x is a variable.

It is useful to replace the variables t' and t" in Eq. [1] respectively by the constant times of the SE sequence TR and TE, and to treat the two time constants T_1 and T_2 in Eq. [1] as variables. This changes Eq. [1] to:

$$S = K\rho_m\left(1-e^{-TR/T_1}\right)e^{-TE/T_2} \quad [2]$$

or:

$$S = KS_{\rho_m}\cdot S_{T_1}\cdot S_{T_2} \quad [3]$$

where the signals for the three segments S_{ρ_m}, S_{T_1}, and S_{T_2} are given by:

$$S_{\rho_m} = \rho_m \quad [4]$$

$$S_{T_1} = 1-e^{-TR/T_1} \quad [5]$$

$$S_{T_2} = 1-e^{-TE/T_2} \quad [6]$$

The second and third segments in Eq. [2] are of the forms $y = 1 - e^{-1/x}$ and $y = e^{-1/x}$ respectively, since T_1 and T_2 are now variables. These forms are quite different from the forms $y = 1 - e^{-x}$ and $y = e^{-x}$ shown in the second and third segments of the Bloch equations in Eq. [1].

The three segments in Eqs. [2-6] have the features of a linear or exponential high pass filter for ρ_m [depending on whether the X axis is linear or natural logarithmic (ln)], a low pass filter for T_1 (i.e., low values of T_1 pass) and a high

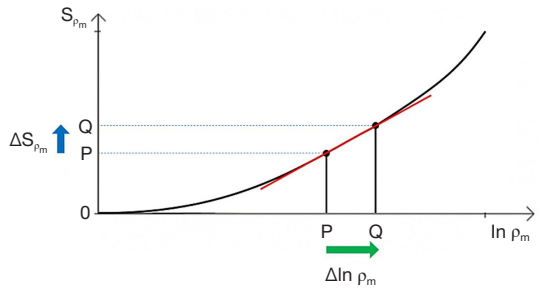

Figure 2 SE sequence. ρ_m-filter with ln ρ_m X axis. It is an exponential filter. The positive increase in ρ_m from P to Q (horizontal green arrow) $\Delta \ln \rho_m = \Delta\rho_m/\rho_m$ is multiplied by the positive slope of the filter (red line) to give positive contrast (vertical blue arrow). $\Delta S_{\rho_m} = C_{ab}$. SE, spin echo.

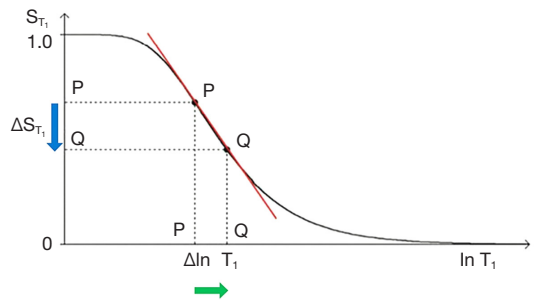

Figure 3 SE sequence. T_1-filter with a ln T_1 X axis. It is a low pass filter. The positive increase in T_1 from P to Q (horizontal green arrow) $\Delta \ln T_1 = \Delta T_1/T_1$ is multiplied by the negative slope of the filter (red line) to give negative contrast (vertical blue arrow). $\Delta S_{T_1} = C_{ab}$. ΔS_{T_1} may be positive or negative. $\Delta \ln T_1$ may also be positive or negative. SE, spin echo.

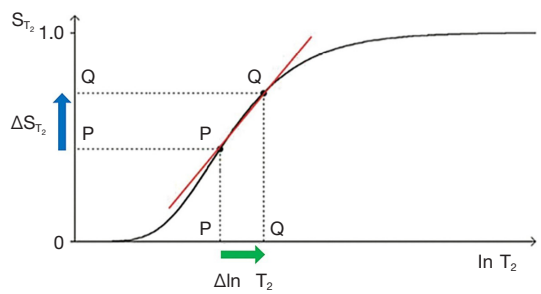

Figure 4 SE sequence. T_2-filter with a ln T_2 X axis. It is a high pass filter. The positive increase in T_2 from P to Q (horizontal green arrow) $\Delta \ln T_2 = \Delta T_2/T_2$ is multiplied by the positive slope of the filter (red line) to give positive contrast (vertical blue arrow). $\Delta S_{T_2} = C_{ab}$. SE, spin echo.

pass filter for T_2 (i.e., high values of T_2 pass) (*Figures 2-4*).

The signal levels on images are given by Eqs. [2-6] for S_{ρ_m}, S_{T_1}, and S_{T_2}, and correspond to the signal or brightness of tissues seen on images.

Eqs. [2-6] can be plotted using ln X axes. When using a linear axis, changes in x (i.e., changes in ρ_m, T_1, or T_2) are absolute differences in TPs. When using a ln X axis as in *Figures 2-4*, small changes in x (i.e., Δln ρ_m, Δln T_1, and Δln T_2) represent fractional changes in TPs because for small differences in x, $\Delta \ln x = \Delta x/x$.

Figure 2 shows a ρ_m-filter in which the positive change in ρ_m Δln ρ_m from P to Q along the X axis (horizontal green arrow) is multiplied by the positive slope of the ρ_m-filter (red line) to give the positive change in signal ΔS_{ρ_m} from P to Q along the Y axis (vertical blue arrow). The change in signal ΔS_{ρ_m} is the absolute contrast C_{ab}.

With the T_1-filter shown in *Figure 3*, the positive change in T_1 Δln T_1 from P to Q along the X axis (horizontal green arrow) is multiplied by the negative slope of the T_1-filter (red line) to produce a negative change in signal ΔS_{T_1} from P to Q along the Y axis (vertical blue arrow). The negative change ΔS_{T_1} is the negative contrast C_{ab}.

The equation for C_{ab} for small changes in ΔT_1 and ΔS_{T_1} using a linear X axis is:

$$C_{ab} = \Delta S_{T_1} = \frac{\partial S_{T_1}}{\partial T_1} \cdot \Delta T_1 \quad [7]$$

where $\frac{\partial S_{T_1}}{\partial T_1}$ is the first partial derivative of the T_1-filter with respect to T_1, which is the slope of the T_1-filter, $\cdot$ = multiplied, and ΔT_1 is the change in T_1 using a linear X axis.

Using a ln X axis, as in *Figure 3* and noting that $\Delta \ln T_1 = \frac{\Delta T_1}{T_1}$ for small changes in T_1, and that $\frac{dy}{d(\ln x)} = x\frac{dy}{dx}$, where x is a variable, Eq. [7] becomes:

$$C_{ab} = \Delta S_{T_1} = \frac{\partial S_{T_1}}{\partial \ln T_1} \cdot \frac{\Delta T_1}{T_1} \quad [8]$$

where $\frac{\partial S_{T_1}}{\partial \ln T_1}$ is the slope of the T_1-filter. This is the first partial derivative of the T_1-filter with respect to $\ln T_1$ (when using a ln X axis). $\cdot$ = multiplied, and $\frac{\Delta T_1}{T_1}$ is the fractional change in T_1 as shown in *Figure 3*.

For the T_2-filter (*Figure 4*), the positive change in T_2 $\Delta \ln T_2 = \frac{\Delta T_2}{T_2}$ from P to Q along the X axis (horizontal green

arrow) is multiplied by the positive slope of the T_2-filter (red line) and this results in the positive change in signal ΔS_{T_2} from P to Q along the Y axis and positive contrast $C_{ab} = \Delta S_{T_2}$.

Putting the second derivative of the T_1- and T_2-filters to zero yields the T_1 or T_2 value where the slope of the T_2-filter, and therefore the contrast, is highest. For the T_1- and T_2-filters, the slope is greatest at TR = T_1 and TE = T_2 when using a ln X axis, and at TR = $2T_1$ and TE = $2T_2$ when using a linear X axis.

For fractional contrast $C_{fr} = \Delta S/S$ (rather than absolute contrast $C_{ab} = \Delta S$), Eqs. [7,8] are divided by S_{T_1} and S_{T_2} respectively for non-zero values of S_{T_1} and S_{T_2}.

So, for T_1 using a ln X axis:

$$C_{fr} = \frac{1}{S_{T_1}} \frac{\partial S_{T_1}}{\partial \ln T_1} \cdot \frac{\Delta T_1}{T_1} \quad [9]$$

and for T_2 using a ln X axis:

$$C_{fr} = \frac{1}{S_{T_2}} \frac{\partial S_{T_2}}{\partial \ln T_2} \cdot \frac{\Delta T_2}{T_2} \quad [10]$$

The SE sequence (multivariate model)

TP-filters can be considered separately [i.e., a univariate model for each TP (i.e., ρ_m, T_1, and T_2) alone, as in the previous section], or be combined in a multivariate model of the SE sequence as in this section. The multivariate model in *Figure 5* shows the contributions to contrast of the change in each TP and the corresponding sequence weighting for each TP i.e., ρ_m, T_1, and T_2 (vertical blue arrows for each TP). The overall contrast (vertical blue arrow on the right) is the algebraic sum of the contrasts produced by each TP.

From Eqs. [3-6] for small change in $\Delta\rho_m$, ΔT_1, and ΔT_2, and using a ln X axis, the product rule from differential calculus gives:

$$\Delta S = \frac{\partial S_{\rho_m}}{\partial \ln \rho_m} S_{T_1} S_{T_2} \cdot \frac{\Delta \rho_m}{\rho_m} + S_{\rho_m} \frac{\partial S_{T_1}}{\partial \ln T_1} S_{T_2} \cdot \frac{\Delta T_1}{T_1} + S_{\rho_m} S_{T_1} \frac{\partial S_{T_2}}{\partial \ln T_2} \cdot \frac{\Delta T_2}{T_2} \quad [11]$$

Normalizing Eq. [11] by dividing it by S and using Eq. [3], for non-zero values of S, S_{ρ_m}, S_{T_1}, and S_{T_2}, C_{fr} is given by:

$$C_{fr} = \frac{\Delta S}{S} = \frac{1}{S_{\rho_m}} \frac{\partial S_{\rho_m}}{\partial \ln \rho_m} \cdot \frac{\Delta \rho_m}{\rho_m} + \frac{1}{S_{T_1}} \frac{\partial S_{T_1}}{\partial \ln T_1} \cdot \frac{\Delta T_1}{T_1} + \frac{1}{S_{T_2}} \frac{\partial S_{T_2}}{\partial \ln T_2} \cdot \frac{\Delta T_2}{T_2} \quad [12]$$

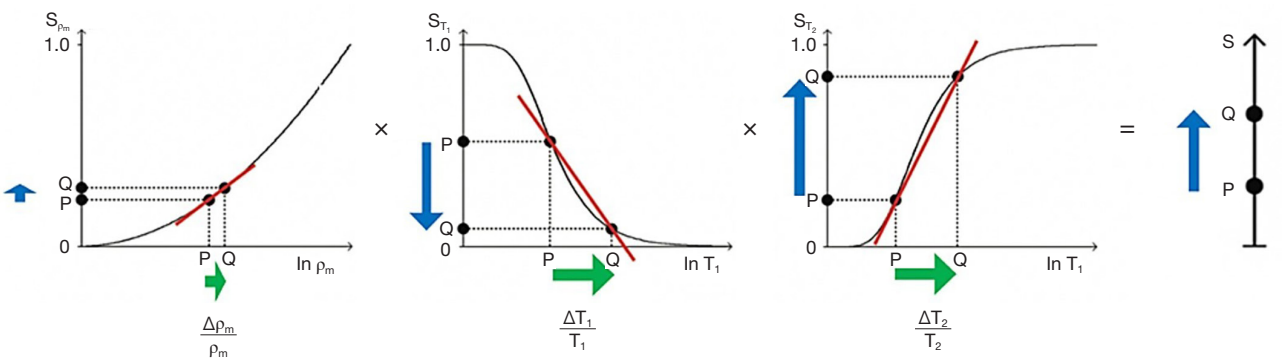

Figure 5 SE sequence with combination of ρ_m-, T_1-, and T_2-filters (multivariate model). Increases in $\Delta\rho_m/\rho_m$, $\Delta T_1/T_1$, and $\Delta T_2/T_2$ (horizontal green arrows) are multiplied by the slopes of their respective TP-filters (red lines) to produce positive, negative, and positive ρ_m, T_1, and T_2 contrasts from their respective TP-filters (vertical blue arrows with each filter). The overall fractional contrast (vertical blue arrow on right) is the algebraic sum of the fractional contrasts produced by each of the three TP-filters (blue arrows with ρ_m-, T_1-, and T_2-filters). SE, spin echo; TP, tissue property.

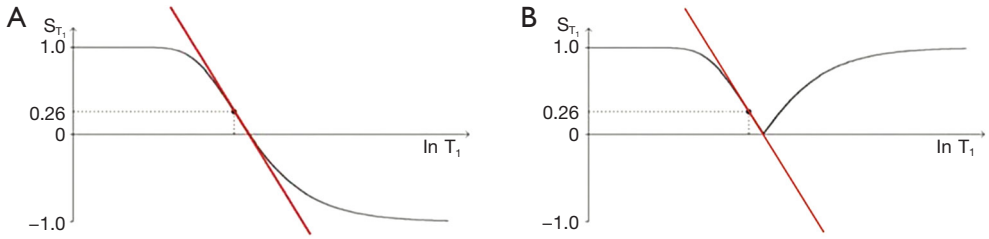

Figure 6 IR T_1-filters with phase-sensitive (A) and magnitude reconstruction (B) using ln T_1 axes. (A) A low pass T_1-filter; (B) a notch T_1-filter. (A) Both positive and negative values for S_{T_1} whereas in (B) negative values are "reflected" across the X axis and become positive. The maximum slopes of the T_1-filters are shown as red lines, and are negative in both cases. IR, inversion recovery.

Thus, the contributions of the TPs to the overall fractional contrast C_{fr} are, for each TP, its sequence weighting multiplied by the fractional change in the TP.

This can be expressed as:

$$C_{fr} = \sum_{TP} \frac{1}{S_{TP}} \frac{\partial S_{TP}}{\partial \ln TP} \cdot \frac{\Delta TP}{TP} \quad [13]$$

where $1/S_{TP}\ S_{TP}/\partial \ln$ TP is the sequence weighting for the TP which is the slope of the TP-filter. ΔTP/TP is the fractional change in the TP. The TPs are ρ_m, T_1, and T_2 for the SE sequence. Eq. [13] is one form of the CCT of MRI. Using a ln X axis, it states that the contrast for each TP is the normalized first partial derivative with respect to ln TP multiplied by the fractional change in TP. The total fractional contrast C_{fr} is the algebraic sum of the contributions to contrast from each TP.

When a single TP such as T_1 is used, the contributions to T_1 contrast from the different parts of the sequence need to be of the same sign to achieve overall contrast. With two different TPs, such as T_1 and T_2, their fractional contrasts also need to be of the same sign to achieve overall synergistic contrast. If one TP contrast is negative and the other is positive a reduction in overall C_{fr} results.

The IR sequence

The IR sequence has an additional T_1-filter (segment) to those of the SE sequence shown in *Figure 6*. This IR T_1-filter is:

$$S_{T_I} = \left(1 - 2e^{-TI/T_1}\right) \quad [14]$$

where S_{T_I} is the signal from the T_1-filter, TI in the inversion time and T_1 is the longitudinal relaxation time. The IR T_1-filter is shown in phase-sensitive (ps) reconstructed form in *Figure 6A* where it is a low pass filter, and in magnitude (m) reconstructed form in *Figure 6B* where it is a notch filter.

When TI is increased, the T_1-filter shifts to the right as shown for the m form of the IR T_1-filter in *Figure 7*. *Figure 7A* (left) shows the IR T_1-filter with a short TI (TI_s) (e.g., the STIR sequence) for the brain where gray matter (G) has a higher signal than white matter (W). The slope of the T_1-filter between W and G is strongly positive.

When TI is increased to a TI_i as in *Figure 7B* (center) the T_1-filter is shifted to the right. W and G are fixed in the same position on the ln X axis, and W now has a higher signal than G. The slope of the T_1-filter between W and G is strongly negative.

When TI_l is increased further with a long TI_l, the filter is displaced further to the right, as in *Figure 7C* (right). W has a slightly higher signal than G, and the slope of the T_1-filter between them is negative but of smaller size than in *Figure 7B*. The sequence weighting of the T_1-filter, which is the slope or first partial derivative of the filter, is highly positive in (*Figure 7A*), highly negative in (*Figure 7B*) and slightly negative in (*Figure 7C*) using a TI_s (*Figure 7A*), a TI_i (*Figure 7B*), and a TI_l (*Figure 7C*) respectively.

Note that when the IR sequence TR is much greater than T_1, the other T_1-filter ($1 - e^{-TR/T_1}$) becomes ~1 and the principal determinant of T_1 contrast is the ($1 - 2e^{-TI/T_1}$) T_1-filter.

MASDIR sequences

Classification of MASDIR sequences

A classification of MASDIR sequences is shown in *Table 1*. They are separated into: (i) multiplied, (ii) added, (iii) subtracted, and (iv) divided groups (left column). More than one of the arithmetical operations (multiplication, addition, subtraction, and division) may be performed in a single sequence.

(i) MIR sequences: MIR sequences include the DIR

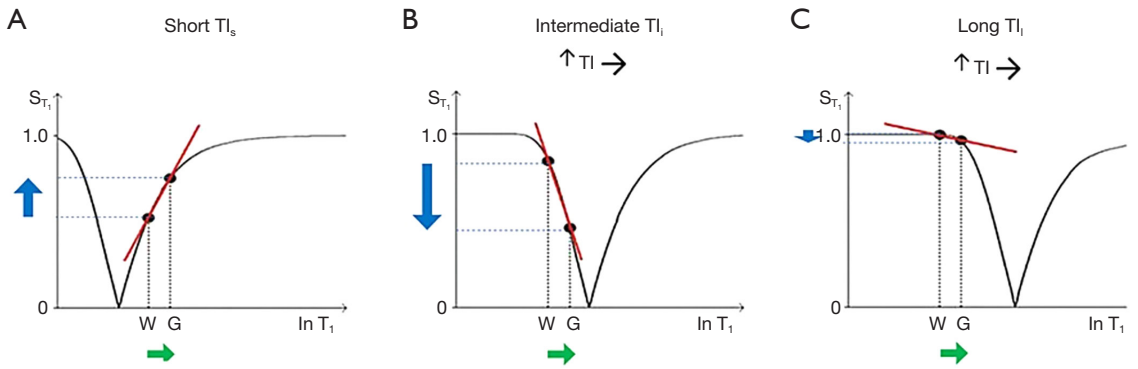

Figure 7 The long TR IR sequence. T_1-filters for TI_s (A), TI_i (B), and TI_l (C) values. The positions of W and G are the same for each (TI). TI is increased from TI_s (A) to TI_i (B) and increased further to TI_l (C). The increase in T_1 from W to G (horizontal green arrows) is multiplied by the relevant slopes of the T_1-filters (red lines) and produces strongly positive, strongly negative, and mildly negative contrast in (A-C) respectively (vertical blue arrows), as TI is increased from left to right. TI_s, short TI; TI, inversion time; TI_i, intermediate TI; TI_l, long TI; W, white matter; G, gray matter; TR, repetition time; IR, inversion recovery.

Table 1 Classification of MASDIR sequences

Category	Examples of sequences (abbreviations)	Examples of sequences (fuller versions)
MIR	dIR	Double inversion recovery
	MP2RAGE (also added in denominator)	Magnetization prepared 2 rapid acquisition gradient echo
AIR	AIR	Added inversion recovery
SIR	SIR	Subtracted inversion recovery
	rSIR	Reverse subtracted inversion recovery
dIR	dSIR (also subtracted, and added in denominator)	Divided subtracted inversion recovery
	drSIR (also subtracted, and added in denominator)	Divided reverse subtracted inversion recovery
	FLAWS-hc (also subtracted, and added in denominator)	Fluid and white matter suppression high contrast
	FLAWS-hco (also subtracted, and added in denominator)	Fluid and white matter suppression high contrast opposite

MASDIR, multiplied, added, subtracted and/or divided inversion recovery; MIR, multiplied inversion recovery; dIR, double IR.

and MP2RAGE sequences as described in the "Introduction" section;

(ii) Added IR (AIR) sequences: one type of AIR sequence adds two magnitude (m) reconstructed sequences with different TIs and can be used with subtraction and division [see the (iv) section below];

(iii) SIR sequences: the SIR and reverse rSIR sequences are included in this group. The SIR sequence uses the subtraction: shorter TI image minus longer TI image, and the rSIR sequence uses the reverse (r) subtraction: longer TI image minus shorter TI image;

(iv) Divided IR (dIR) sequences (dSIR and drSIR): a central issue with division of IR sequences is the behavior of the T_1-filter if, or when, the denominator takes a value of zero. This potentially leads to infinite values of the T_1-filter. Even if zero values are avoided, there may be uncertain values when the denominator approaches zero and division becomes unreliable as a consequence of noise and/or artifacts.

The problem can largely be avoided in the case of two magnitude IR images with different TIs (e.g., SIR and rSIR images) by making the denominator the addition (or sum) of the signals from the two images. Because the T_1-filters have different TIs, when using magnitude reconstruction addition of them in the denominator is non-zero.

When the numerator is two SIR images, division

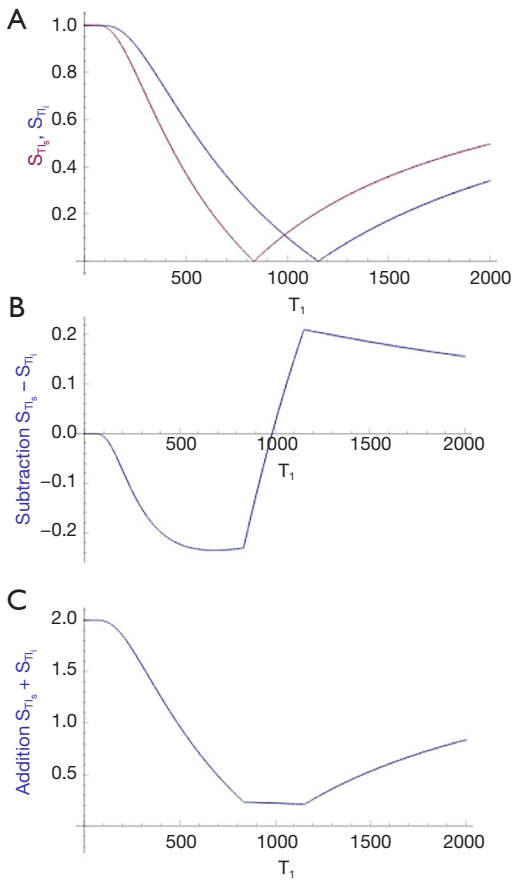

Figure 8 SIR and AIR T_1-filters. T_1 is shown along the X axis in ms. (A) The TI_s T_1-filter (pink) and TI_i T_1-filter (blue); (B) the subtraction $\left(S_{TI_s} - S_{TI_i}\right)$ IR or SIR T_1-filter; (C) the addition $\left(S_{TI_s} + S_{TI_i}\right)$ IR or AIR T_1-filter. In (B) the slope of the curve in the mD is about double that of the S_{TI_s} T_1-filter [pink in (A)]. In (C) the signal at T_1=0 is doubled to 2.0, and the signal in the mD is reduced to about 0.20 in the nearly linear, slightly downward sloping central part of the AIR T_1-filter (i.e., in the mD). TI_s, short TI; TI, inversion time; TI_i, intermediate TI; SIR, subtracted inversion recovery; AIR, added inversion recovery; IR, inversion recovery; mD, middle domain.

normalizes the sequence so that to a first approximation, the effects of ρ_m and T_2 are eliminated. As a result, dSIR and drSIR images are essentially T_1 maps.

The dSIR T_1-bipolar filter

Two magnitude IR T_1-filters with different TIs (TI_s and TI_i) are shown in *Figure 8A*. They are subtracted (TI_s minus TI_i) to give the SIR T_1-filter in *Figure 8B*. The SIR T_1-filter has a steep positive slope in the X axis region between the T_1s corresponding to the two nulling TIs, i.e., in the mD. Subtraction of the negative slope of the TI_i T_1-filter from the positive slope of the TI_s T_1-filter produces a synergistic near doubling of the positive slope in the mD of the SIR T_1-filter. The width of the mD is determined by the difference in TI between the two filters, ΔTI. Small ΔTIs give a narrow mD and large ΔTIs give a wide mD. ΔTI is the difference between the two TIs i.e., first reference, baseline or targeted tissue TI (mostly the nulling TI of the normal tissue) and the second TI chosen to match the targeted change in the sign and size of T_1. By convention ΔTI is taken as the second TI minus the first TI and may be positive or negative. ΔTI is positive for dSIR T_1-filters which have a positive slope and is negative for drSIR T_1-filters which have a negative slope (see later). If ΔTI is the same sign as the change in T_1 (ΔT_1) contrast is positive. If ΔTI and ΔT_1 are of opposite sign, contrast is negative. With the dSIR T_1-filter targeted at normal appearing white matter and small increases in T_1, ΔTI is the longer TI chosen to allow for an increase in T_1 in disease, minus the shorter TI nulling normal white matter. Thus ΔTI is positive and so is ΔT_1. This results in positive contrast.

The two T_1-filters in *Figure 8A* can also be added as an AIR T_1-filter which is shown in *Figure 8C*. There are higher signals and higher slopes outside of the mD. Within the mD there is a generally low signal with a nearly linear slightly downward sloping curve.

Figure 9A shows the dSIR T_1-bipolar filter in which the SIR T_1-filter in *Figure 8B* is divided by the AIR T_1-filter in *Figure 8C*. The dSIR T_1-bipolar filter shows a very high positive slope in its mD. The sloping mD in *Figure 8B* (the SIR T_1-filter) was divided by the fractional value mD in the AIR T_1-filter to greatly increase the slope shown in the mD of the dSIR T_1-filter.

Figure 9B compares the contrast from the TI_s T_1-filter, S_{TI_s} (pink) which is that of a conventional IR sequence such as MP-RAGE, to that from a SIR T_1-filter (blue). For the same positive change in T_1 (positive horizontal green arrow in the mD, ΔT_1) the vertical pink and blue arrows on the right show that the positive contrast produced by the SIR T_1-filter is about double that produced by the S_{TI_s} T_1-filter.

Figure 9C compares the contrast produced by a TI_s T_1-filter, S_{TI_s} (pink) to that from a dSIR T_1-bipolar filter (blue). For the same positive change in T_1 (positive horizontal green arrow in the mD, ΔT_1) the dSIR T_1-bipolar filter generates about 10 times the positive contrast produced by the S_{TI_s} T_1-filter (vertical pink and blue arrows on the

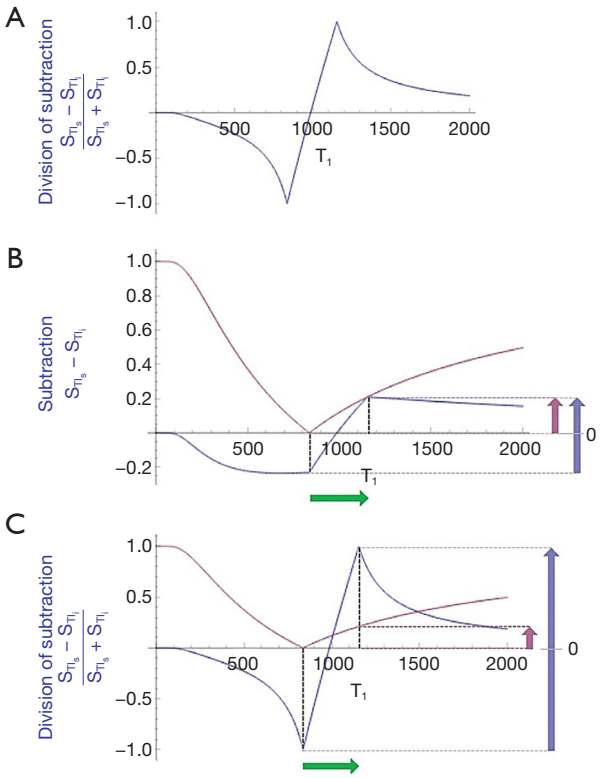

Figure 9 dSIR T_1-bipolar filter (A), comparison of the S_{TI_s} T_1-filter with the SIR T_1-filter (B), and comparison of the S_{TI_s} T_1-filter with the dSIR T_1-bipolar filter (C) for an increase in T_1 (ΔT_1) in the mD. T_1 is shown along the X axis in ms. In (A) division of the subtraction $(S_{TI_s} - S_{TI_i})$ T_1-filter by the addition $(S_{TI_s} + S_{TI_i})$ AIR T_1-filter gives $(S_{TI_s} - S_{TI_i}) / (S_{TI_s} + S_{TI_i})$ or SIR/AIR which is the dSIR T_1-bipolar filter. The dSIR T_1-bipolar filter shown in (A,C) has maximum and minimum values of 1 and −1 respectively and has a steeply positive slope in its mD. (B) The increase in signal (i.e., contrast) for the increase in T_1 within the mD (positive horizontal green arrow, ΔT_1) is about 0.20 for the S_{TI_s} T_1-filter and about 0.42 for the SIR T_1-filter. This represents an increase in positive contrast for the SIR T_1-filter compared to the S_{TI_s} T_1-filter of about two (right vertical pink and blue arrows). (C) The contrast produced by in the S_{TI_s} T_1-filter by the change in T_1 (positive horizontal green arrow, ΔT_1) is about 0.20 as also shown in (B), and the contrast produced by the dSIR T_1-bipolar filter is 2.0 representing an increase in positive contrast of about 10 times (right vertical pink and blue arrows). TI_s, short TI; TI, inversion time; TI_i, intermediate TI; dSIR, divided subtracted inversion recovery; SIR, subtracted inversion recovery; AIR, added inversion recovery; mD, middle domain.

right). This follows directly from the CCT i.e., increasing the slope of the T_1-filter increases the contrast produced by the same change in T_1, ΔT_1.

As the second TI is moved closer to the first TI, the magnitude of ΔTI decreases, the dSIR T_1-bipolar filter becomes steeper in its mD, and the T_1 dependent contrast generated increases for the same change in T_1 (providing the change is within the mD). This is documented in *Table 2*. In this table, ΔTI is negative. As its magnitude decreases from 90% to 13% of the initial TI, the ratio of the contrast produced by the dSIR T_1-bipolar filter to that produced by the conventional IR T_1-filter increases from 5 to 20.

Figure 9C also shows sequence targeting. The T_1 X axis has low, middle and high domains separated by the vertical dashed lines. The T_1-filter of the conventional IR sequence (pink) has a mostly non-zero slope and is sensitive to changes in T_1 in all three domains including T_1 values from near zero to the maximum value of T_1 shown.

The dSIR T_1-bipolar filter (blue) has a generally similar slope to the conventional IR T_1-filter in the first domain and in the third domain (though of opposite sign there). In the mD however, the slope of the dSIR T_1-bipolar filter is about 10 times higher than that of the conventional IR filter. As a result, the positive contrast produced by it is 10 times greater for the same change in T_1. This increase in positive contrast is confined to the mD. To exploit the increased contrast, TI_s need to be chosen to place the mD of the dSIR T_1-bipolar filter in a position to target the change in T_1. To do this for normal white matter, the first TI of the dSIR T_1-bipolar filter needs to correspond to the normal value of T_1 of white matter to achieve nulling. The second TI needs to be chosen to target the sign and size of the change in T_1 that is expected. In *Figure 9C* the dSIR T_1-bipolar filter is targeted firstly to null normal tissue, and secondly to produce positive contrast from the positive change in T_1 from normal (positive horizontal green arrow, ΔT_1). The size of ΔTI is sufficient to include the change in T_1 i.e., the extent of the horizontal green arrow.

If the change in T_1 (ΔT_1) is negative as in *Figure 10* (negative horizontal green arrow, ΔT_1), and ΔTI is positive (as for the dSIR T_1-bipolar filter), the resulting contrast is negative (vertical blue arrow on the right). It is about 10 times the size of the contrast produced by the conventional IR sequence (vertical pink arrow on right).

The drSIR T_1-bipolar filter

Figure 11A shows the same two magnitude IR T_1-filters

Table 2 TI_s, TI_i, ΔTI, S_{TI_s} contrast at TI_i, S_{dSIR} contrast at TI_i, and ratio S_{dSIR} contrast/S_{TI_s} contrast

TI_s (ms)	TI_i (ms)	ΔTI		S_{TI_s} contrast	S_{dSIR} contrast	Ratio S_{dSIR} contrast/S_{TI_s} contrast
		ms	%			
580	1,100	520	90	0.40	2.0	5
580	840	260	45	0.25	2.0	8
580	710	130	22	0.15	2.0	13
580	655	75	13	0.10	2.0	20

ΔTI is the second TI (1,100–655 ms) minus the first TI (580 ms) for the dSIR T_1-bipolar filter, and is positive. As TI_i is reduced from 1,100 ms (first row) to 655 ms (fourth row), the mD narrows and the magnitude of ΔTI decreases from 90% (first row) to 13% (fourth row). As the mD narrows and the magnitude of ΔTI decreases, the ratio dSIR contrast/S_{TI_s} contrast increases from 5 (first row) to 20 (fourth row). TI_s, short TI; TI, inversion time; TI_i, intermediate TI; dSIR, divided subtracted inversion recovery; mD, middle domain.

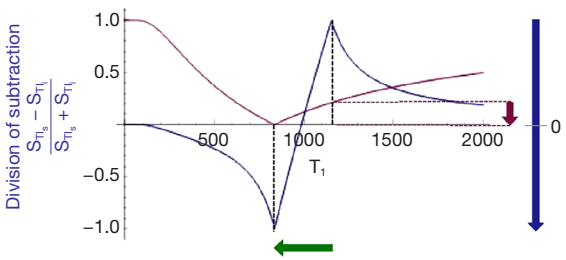

Figure 10 dSIR T_1-bipolar filter shown in *Figure 9C* (blue) and S_{TI_s} T_1-filter (pink) for a decrease in T_1 (not an increase in T_1 as in *Figure 9C*). T_1 is shown along the X axis in ms. The decrease in T_1 (negative horizontal green arrow, ΔT_1) results in negative contrast for both the conventional IR T_1-filter (negative vertical pink arrow) and the dSIR T_1-bipolar filter (negative vertical blue arrow). The contrast is opposite in sign to what is seen in *Figure 9C*. The negative contrast is about 10 times greater for the dSIR T_1-bipolar filter compared with the conventional IR T_1-filter. TI_s, short TI; TI, inversion time; TI_i, intermediate TI; dSIR, divided subtracted inversion recovery; IR, inversion recovery.

with signals S_{TI_s} and S_{TI_i} as in *Figure 8A*. In *Figure 11B* the r subtraction rSIR T_1-filter is shown (i.e., S_{TI_i} minus S_{TI_s}). This has a negative slope in the mD. *Figure 11C* shows addition of the two original IR T_1-filters to give the AIR T_1-filter. *Figure 12A* shows the rSIR T_1-filter in *Figure 11B* divided by the AIR T_1-filter in *Figure 11C* which gives the drSIR T_1-bipolar filter. This has a steep negative slope in the mD and a negative ΔTI. *Figure 12B* shows a comparison of the S_{TI_i} T_1-filter (pink) with the rSIR T_1-filter (blue) for a decrease in T_1 as may be seen with hemorrhage, iron accumulation and GBCA administration (negative horizontal green arrow, ΔT_1). The positive contrast produced by the rSIR T_1-filter is about twice that of the S_{TI_i} T_1-filter (vertical pink and blue arrows on right). *Figure 12C* shows a comparison of the S_{TI_i} T_1-filter (pink) with the drSIR T_1-bipolar filter (blue) for the same negative change in T_1 (negative horizontal green arrow, ΔT_1). The positive contrast produced by the drSIR T_1-bipolar filter is about 10 times greater than that obtained with the S_{TI_i} T_1-filter (vertical pink and blue arrows on right). In this case, the drSIR T_1-bipolar filter is targeted to produce positive contrast from the negative change in T_1.

If the change in T_1 (ΔT_1) is positive, as in *Figure 13*, then the negative ΔTI of the drSIR T_1-bipolar filter, coupled with the positive ΔT_1 means that the contrast is negative (vertical blue arrow on right). It is about 10 times the size of the negative contrast produced by the conventional IR sequence (vertical pink arrow on right).

Synergistic contrast MRI (scMRI)

Synergistic contrast arises in two main ways:

(i) A single TP can be used twice or more in a sequence to increase contrast. For example, changes in T_1 can be used in the T_1 dependent TR segment of an IR sequence as well as the T_1 dependent TI segment. Changes in T_1 are also used twice in the SIR sequence when employing the subtraction: TI_s T_1-filter minus TI_i T_1-filter. T_1 changes are also used twice in the rSIR T_1-filter with the reverse subtraction. The synergistic T_1 contrast from the SIR and rSIR sequences can be increased further by using T_1 changes 3–4 times by employing division with them as for the dSIR and drSIR sequences;

(ii) Two or more different TPs can also be used to produce synergistic contrast as was first described

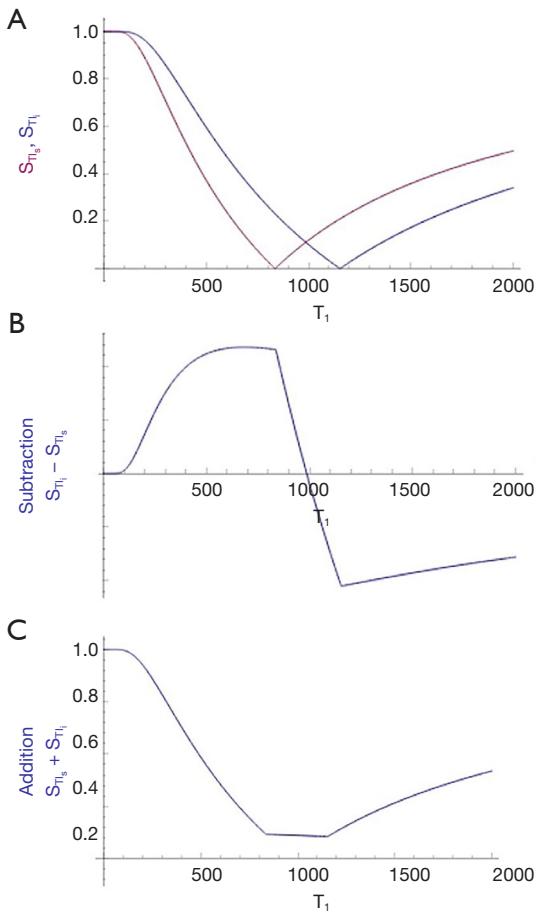

Figure 11 rSIR and AIR T_1-filters. T_1 is shown along the X axis in ms. (A) The TI_s (pink) and TI_i (blue) T_1-filters; (B) the subtraction $\left(S_{TI_i} - S_{TI_s}\right)$ or rSIR T_1-filter; (C) the addition $\left(S_{TI_s} + S_{TI_i}\right)$ or AIR T_1-filter. In (B) the slope of the filter in the mD is negative and about double that of the S_{TI_i} T_1-filter. In (C) the signal at T_1=0 is doubled to 2.0, and the signal in the mD it is reduced to about 0.20 as shown in the nearly linear slightly downward sloping central part of the AIR T_1-filter (i.e., in the mD). TI_s, short TI; TI, inversion time; TI_i, intermediate TI; rSIR, reverse subtracted inversion recovery; AIR, added inversion recovery; mD, middle domain.

with the STIR sequence in 1985 (7). Clinical pulse sequences have a basic structure consisting of ρ_m, T_1, and T_2-filters as seen in SE sequences. There are additional options which can be added such as those for T_1 dependent inversion pulses and apparent diffusion coefficient (D*) sensitization. In many circumstances ρ_m is a minor determinant of contrast and T_1, T_2, and D* are major determinants.

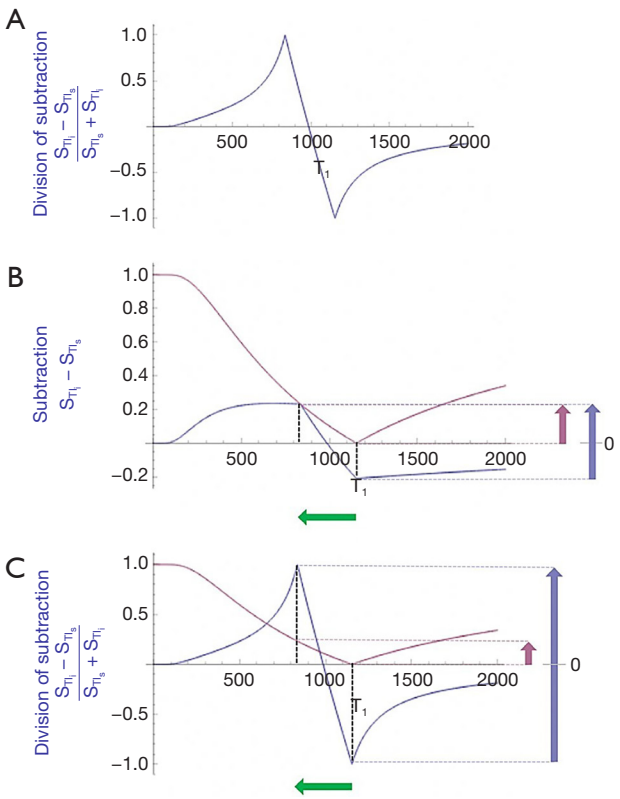

Figure 12 drSIR T_1-bipolar filter (A), comparison of the S_{TI_i} T_1-filter with the rSIR T_1-filter (B), and comparison of the S_{TI_i} T_1-filter with the drSIR T_1-bipolar filter (C) for a decrease in T_1 in the mD. T_1 is along the X axis in ms. In (A) division of the subtraction rSIR $\left(S_{TI_i} - S_{TI_s}\right)$ T_1-filter by the AIR T_1-filter gives $\left(S_{TI_i} - S_{TI_s}\right)/\left(S_{TI_s} + S_{TI_i}\right)$ or rSIR/AIR which is the drSIR T_1-bipolar filter. The drSIR T_1-bipolar filter in (A,C) has maximum and minimum values of 1 and −1 respectively and has a steeply negative slope in its mD. In (B) the increase in signal (i.e., contrast) for the decrease in T_1 within the mD (negative horizontal green arrow, ΔT_1) is about 0.20 for the S_{TI_i} T_1-filter (positive vertical pink arrow) and about 0.42 for the rSIR T_1-filter (vertical blue arrow). This represents an increase in contrast for the rSIR T_1-filter compared with the S_{TI_s} T_1-filter of about two (right vertical pink and blue arrows). In (C) for the same decrease in T_1 (negative horizontal green arrow, ΔT_1) the contrast with the S_{TI_i} T_1-filter is about 0.20 as in (B) (vertical pink arrow), and the contrast with the drSIR T_1-bipolar filter is 2.0 (vertical blue arrow) representing an increase in positive contrast of about 10 times. TI_s, short TI; TI, inversion time; TI_i, intermediate TI; drSIR, divided reverse subtracted inversion recovery; rSIR, reverse subtracted inversion recovery; AIR, added inversion recovery; mD, middle domain.

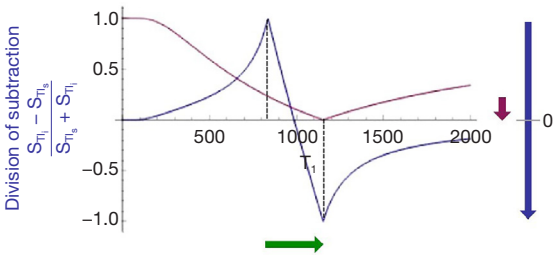

Figure 13 drSIR T_1-bipolar filter (blue) and conventional IR T_1-filter (pink) as shown in *Figure 12C*, but with an increase in T_1, not the decrease in T_1 shown in *Figure 12C*. T_1 is shown along the X axis in ms. The increase in T_1 (positive horizontal green arrow, ΔT_1) results in negative contrast for both the conventional IR T_1-filter (negative vertical pink arrow) and the drSIR T_1-bipolar filter (negative vertical blue arrow). This contrast is of the opposite sign to what is seen in *Figure 12C*. With the drSIR T_1-bipolar filter, the negative contrast is about 10 times greater than with the conventional IR T_1-filter. TI_s, short TI; TI, inversion time; TI_i, intermediate TI; drSIR, divided reverse subtracted inversion recovery; IR, inversion recovery.

The most common change in TPs in disease is concurrent increases in ρ_m, T_1, T_2. In this situation with the SE sequence, the contrast developed by an increase in T_1 is negative while the contrast developed by an increase in T_2 is positive, so that simultaneous increases in T_1 and T_2 produce opposed contrast and the net, or overall, contrast is reduced. To avoid this problem, T_1-weighted SE sequences use a short TE to minimize the opposed T_2 contrast, and T_2-weighted SE sequences use a long TR to minimize the opposed T_1 contrast. The dominant source of contrast in the resulting sequences is then a single TP, i.e., T_1 or T_2 and the sequences are described as T_1-weighted or T_2-weighted respectively. T_1 and T_2 are each used only once to create contrast in both sequences, and so the sequences are not synergistic for T_1 and T_2 contrast.

In particular circumstances, such as certain forms of the STIR and the DIR sequences, the T_1 contrast produced by an increase in T_1 is positive, and so is the T_2 contrast produced by an increase in T_2. The effects of concurrent increases in T_1 and T_2 are therefore synergistic, and typically result in high positive lesion contrast.

The synergistic contrast produced above from (i) a single TP, and/or (ii) two or more different TPs can be supplemented by increasing or decreasing signals from normal tissues and/or fluids. There may be little contrast between high signal lesions and high signal fat, long T_2 tissues, or fluids. Reduction in the normal signal from these tissues or fluids [using the same or different TPs as those used to create the original synergistic contrast in (i) and/or (ii)] can increase the contrast between the high signal lesions and the zero or low signal suppressed tissues and/or fluids.

Contrast at tissue boundaries

In the previous sections of this paper, contrast between two pure voxels each containing a pure sample of a different tissue has been considered, but there has been no reference to the location of the voxels, contrast at boundaries between two voxels, or contrast within transitional regions between the two pure voxels where there are mixed voxels containing mixtures of the two different tissues (i.e., there are partial volume effects).

In general terms, contrast detectability at boundaries between two pure voxels with different values of S can be related to contrast $C_{ab} = \Delta S$ or $C_{fr} = \Delta S/S$ divided by the distance Δx between the two pure voxels. Boundaries are more detectable when contrast is high and Δx is low, and less detectable in the opposite situation, where contrast is low and Δx is high.

In boundary regions between two pure tissues P and Q it is useful to define the tissue fraction (f) which is the proportion of the second tissue Q in a mixed voxel which contains a mixture of both tissues. The proportion of the other tissue P in the mixed voxel is then (1 – f).

The T_1 of a mixture of the two tissues (P and Q) in a voxel can be expressed as a function

$$T_{1P,Q} = \Gamma\left(T_{1P}, T_{1Q}, f\right) \quad [15]$$

where $T_{1P,Q}$ is the T_1 of the mixture, T_{1P} is the T_1 of P, and T_{1Q} is the T_1 of Q.

It is also useful to consider $\frac{\partial f}{\partial x}$ the change in tissue fraction with distance x. This may be gradual and correspond to a low value of $\frac{\partial f}{\partial x}$, or be abrupt and correspond to a higher value of $\frac{\partial f}{\partial x}$.

Using the chain rule from differential calculus, normalized contrast over distance for T_1 is given by:

$$\frac{1}{S_{T_1}} \cdot \frac{\Delta S}{\Delta x} \approx \frac{1}{S_{T_1}} \cdot \frac{dS}{dx} = \frac{1}{S_{T_1}} \cdot \frac{\partial S_{T_1}}{\partial T_1} \cdot \frac{\partial T_1}{\partial f} \cdot \frac{\partial f}{\partial x} \quad [16]$$

where $\frac{1}{S_{T_1}} \cdot \frac{\Delta S}{\Delta x}$ is the change in fractional contrast with

Table 3 Partial derivatives $\frac{\partial S_{T_1}}{\partial T_1}$, $\frac{\partial T_1}{\partial f}$, and $\frac{\partial f}{\partial x}$ which determine T_1-dependent change in signal (or contrast) with distance at boundaries

$\frac{\partial S_{T_1}}{\partial T_1}$ †	$\frac{\partial T_1}{\partial f}$	$\frac{\partial f}{\partial x}$
Increasing T_1 sequence weighting from lower (first row) to higher (fourth row) (below)	Increasing value from lower (first row) to higher (third row) (below)	Increasing value from lower (first row) to higher (second row) (below)
SGE	White matter-gray matter	Gradual
IR	Gray matter-CSF	Abrupt
SIR	White matter-CSF	
dSIR		

†, sequence weighting = slope of T_1-filter. SGE, spoiled gradient echo; IR, inversion recovery; SIR, subtracted inversion recovery; dSIR, divided subtracted inversion recovery; CSF, cerebrospinal fluid.

distance x, S_{T_1} is the T_1-filter signal, $\frac{dS}{dx}$ is a measure of detectable contrast at a boundary, $\frac{\partial S_{T_1}}{\partial T_1}$ is the first partial derivative of S_{T_1} with respect to T_1, i.e., the sequence weighting, $\frac{\partial T_1}{\partial f}$ is the change in T_1 with tissue fraction (f), and $\frac{\partial f}{\partial x}$ is the change in f with distance x (*Table 3*).

Thus, contrast at a boundary depends on the sequence weighting, the change in T_1 with tissue fraction and the change in tissue fraction with distance. The change in tissue fraction with distance may be abrupt in one plane, but gradual in another plane.

At a boundary between two pure tissues, the T_1s of mixed voxels typically span the range of T_1 values between those of the two pure tissues. If the T_1-bipolar filter has a narrow mD so that a T_1 value between those of white and gray matter produces a peak of the T_1-bipolar filter $S_{W,G}$, as in *Figure 14A*, this results in a high signal narrow line at the boundary between white and gray matter. This high signal boundary is inside the brain and is obtained using a narrow mD. If a wide mD is used as in *Figure 14B*, the peak signal $S_{G,CSF}$ occurs at a T_1 between those of gray matter and CSF where there are mixtures of gray matter and CSF in voxels. As a result, the high signal boundary appears outside the brain. A boundary inside the brain is shown in *Figure 15* and one outside the brain is shown in *Figure 16*.

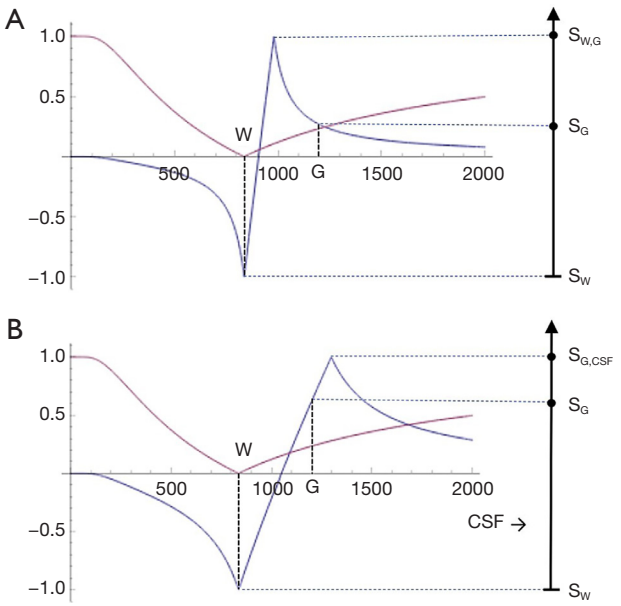

Figure 14 This figure shows a narrow mD T_1-bipolar filter in (A) and a wide mD T_1-bipolar filter in (B). (A) A narrow mD dSIR T_1-bipolar filter (blue) with a mD extending from W to a $T_{1W,G}$ between W and G (blue), and a white matter nulled IR T_1-filter e.g., MP-RAGE (pink). The peak signal ($S_{W,G}$) with the dSIR T_1-bipolar filter appears between W and G along the X axis (in ms) where there is a partial volume effect between W and G producing a $T_{1W,G}$ with a value of T_1 between those of W and G. This results in a high signal $S_{W,G}$ in (A) and corresponds to the high signal boundary between W and G shown in *Figure 15*. (B) A wide mD dSIR T_1-bipolar filter with a mD extending from W to beyond G (blue) and a white matter nulled T_1-filter e.g., MP-RAGE (pink). The peak signal $S_{G,CSF}$ with the dSIR T_1-bipolar filter appears between G and CSF at a T_1 which is higher than that of G and corresponds to a partial volume effect between G and CSF (the T_1 of CSF is off the X axis to the right). This results in a high signal between G and CSF $S_{G,CSF}$ in (B), and corresponds to the high signal at the junction between cortical G and CSF just outside the brain shown in *Figure 16*. W and G are in the same position in (A,B). W, white matter; G, gray matter; CSF, cerebrospinal fluid; mD, middle domain; dSIR, divided inversion recovery; IR, inversion recovery; MP-RAGE, magnetization prepared-rapid acquisition gradient echo.

The width of boundaries seen on dSIR images can be changed by changing the width of the mD. Change from a narrow mD (*Figure 17A*) to an intermediate mD (*Figure 17B*) widens the peak region of the T_1-bipolar filter and increases the width of the boundary. *Figure 18* shows a comparison of an image obtained with a narrow mD

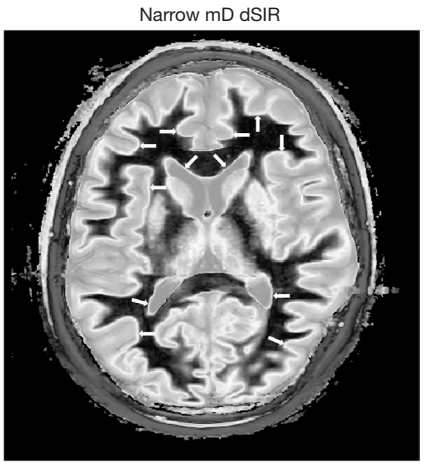

Figure 15 Narrow mD dSIR image with the first TI nulling W and the second TI less than that needed to null G. Narrow high signal boundaries are seen between W and G as well as between W and CSF (white arrows). mD, middle domain; dSIR, divided subtracted inversion recovery; TI, inversion time; W, white matter; G, gray matter; CSF, cerebrospinal fluid.

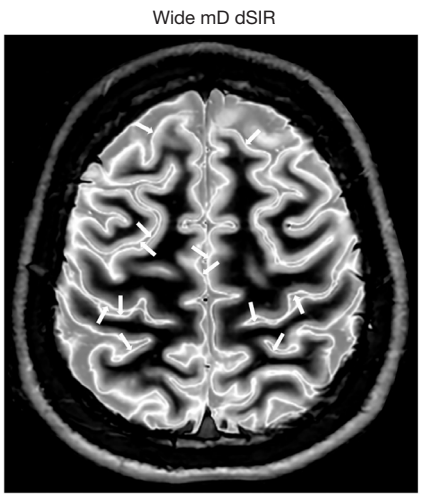

Figure 16 Wide mD dSIR image of the brain using a wide mD with the first TI nulling W and the second TI longer than that needed to null cortical G (TI_s =350 ms, TI_i =800 ms, ΔTI =−130% at 3T). High signal boundaries are seen just outside of the brain between G and CSF (white arrows). mD, middle domain; dSIR, divided subtracted inversion recovery; TI, inversion time; W, white matter; G, gray matter; TI_s, short TI; TI_i, intermediate TI; CSF, cerebrospinal fluid.

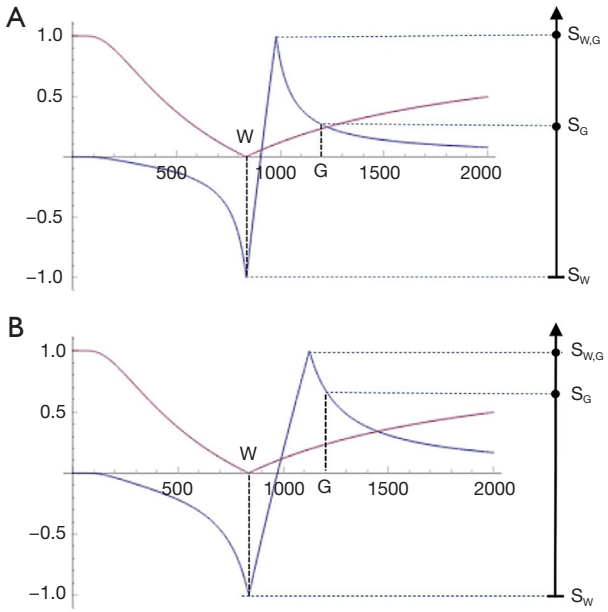

Figure 17 This figure shows a narrow mD T_1-bipolar filter in (A) and an intermediate mD T_1-bipolar filter in (B). In (A) a narrow mD dSIR T_1-bipolar filter (blue) with the first TI nulling W and the second TI nulling a $T_{1W,G}$ between W and G resulting from a mixture of the two tissues is shown. T_1 is shown along the X axis in ms. The pink T_1-filter is that from a white matter nulled IR sequence e.g., MP-RAGE. The signal $S_{W,G}$ is from a mixture of W and G with a T_1 between those of W and G, and is greater than that of the signal from W S_W, and G S_G. It corresponds to the line between W and G seen inside the cortex in *Figure 18A*. In (B) an intermediate mD dSIR T_1-bipolar filter with the first TI nulling W and the second TI nulling a mixture of W and G with a T_1 between W and G with a higher value than the T_1 for nulling the mixture of W and G in (A) is shown. The signal from the mixture $S_{W,G}$ in (B) is greater than that of S_W and S_G. The dSIR T_1-bipolar filter in (B) is wider than the dSIR T_1-bipolar filter in (A) and this corresponds to the wider boundaries between W and G, and between W and CSF seen in *Figure 18B* compared with *Figure 18A*. W and G are in the same position as in *Figure 18A,18B*. W, white matter; G, gray matter; mD, middle domain; dSIR, divided inversion recovery; TI, inversion time; IR, inversion recovery; MP-RAGE, magnetization prepared-rapid acquisition gradient echo; CSF, cerebrospinal fluid.

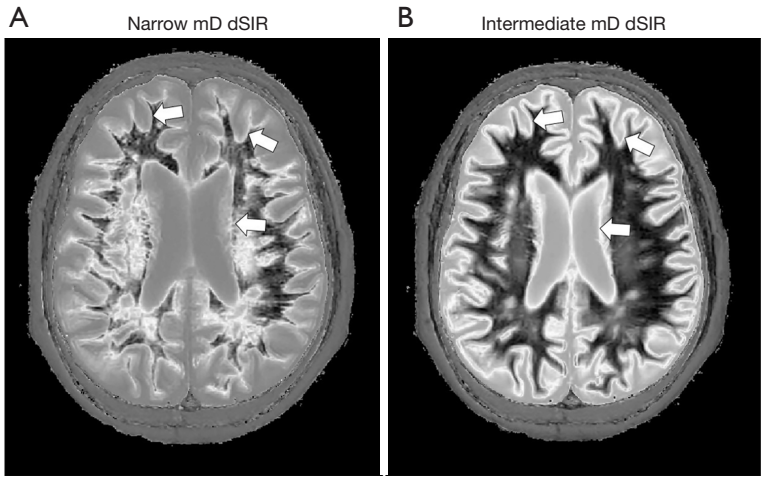

Figure 18 This figure shows a narrow mD dSIR image in (A) and an intermediate mD dSIR image in (B) in a patient with small vessel disease in white matter. In (A) a narrow mD dSIR image (TI_s =540 ms, TI_i =640 ms, ΔTI =18% at 3T) (with about 15 times amplification of contrast) is compared to a standard IR sequence such as MP-RAGE. (B) shows an intermediate mD dSIR image (TI_s =540 ms, TI_i =840 ms, ΔTI =56%). In (A) the slope of the T_1-filter is high, and the high signal boundaries between white matter and gray matter, and between white matter and CSF are narrow (white arrows). In (B) where the slope of the T_1-bipolar filter is lower and its peak is wider, the high signal boundaries between white matter and gray matter, and between white matter and CSF are wider compared to (A) [see corresponding pairs of white arrows in (A,B)]. mD, middle domain; dSIR, divided inversion recovery; IR, inversion recovery; MP-RAGE, magnetization prepared-rapid acquisition gradient echo; TI_s, short TI; TI, inversion time; TI_i, intermediate TI; CSF, cerebrospinal fluid.

(*Figure 18A*) with one obtained using an intermediate mD (*Figure 18B*). The white matter gray matter boundaries are narrow in *Figure 18A* and intermediate in *Figure 18B* (compare the paired white arrows in *Figure 18A,18B*).

In using a dSIR sequence with white matter nulled by the first TI, when the second TI is increased and approaches that for nulling gray matter, the contrast between the high signal boundary and gray matter is reduced. When the second TI becomes the same as that for nulling gray matter, the high signal boundary merges with gray matter. To create a high contrast boundary with gray matter (as well as with white matter) in this situation, the second TI needs to be significantly shorter than the TI which nulls gray matter.

The high signal boundaries between white matter and gray matter on dSIR and drSIR images are characteristic of this type of imaging. Their presence provides validation of the use of T_1-bipolar filters to describe the signal and contrast behavior of the dSIR and drSIR sequences.

T_1 maps

The signals S_s and S_i for two long TR IR magnitude T_1-filters with TI_s and TI_i as shown in *Figures 8A,11A* are respectively given by:

$$S_{TI_s} = 1 - 2e\left(-TI_S / T_1\right) \quad [17]$$

and

$$S_{TI_i} = 1 - 2e\left(-TI_i / T_1\right) \quad [18]$$

Performing the subtraction: magnitude of the IR signal $\left|S_{TI_s}\right|$ in Eq. [17] minus magnitude of the IR signal $\left|S_{TI_i}\right|$ in Eq. [18] gives the signal of the SIR filter S_{SIR} which is equal to $-S_{TI_s} - S_{TI_i}$ i.e.,:

$$S_{SIR} = 2e\left(-TI_S / T_1\right) + 2e\left(-TI_i / T_1\right) - 2 \quad [19]$$

Addition of the magnitudes of the two IR signals $\left|S_{TI_s}\right|$ and $\left|S_{TI_i}\right|$ in Eqs. [17,18] S_{AIR} is equal to $-S_{TI_s} + S_{TI_i}$ i.e.,:

$$S_{AIR} = 2e\left(-TI_S / T_1\right) - 2e\left(-TI_i / T_1\right) \quad [20]$$

Division of the signal of the subtraction T_1-filter S_{SIR} in Eq. [17] by the signal of the addition T_1-filter S_{AIR} in Eq. [18] gives the signal of the S_{dSIR} T_1-filter:

$$S_{dSIR} = \frac{e\left(-TI_S / T_1\right) + e\left(-TI_i / T_1\right) - 1}{e\left(-TI_S / T_1\right) - e\left(-TI_i / T_1\right)} \quad [21]$$

While this expression is accurate, it does not provide easy

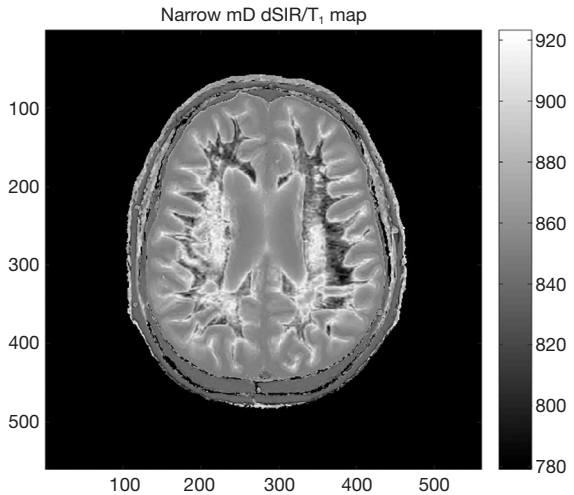

Figure 19 Narrow mD dSIR image/T_1 map (TI_s =540 ms, TI_i =640 ms, ΔTI =18%, TR =6,000 ms) in a patient with small vessel disease showing T_1 values within the mD on the gray-scale at the right. Image dimensions in voxels are shown along the X and Y axes of the image. The T_1 gray-scale covers the mD which is within white matter. The gray-scale shows T_1 values over a range of 144 ms with the dark low signal representing the shorter normal T_1 value of white matter of 780 ms (i.e., 540/ln 2 ms) and higher signal representing abnormal increased T_1 values of white matter up to the maximum of 924 ms (i.e., 640/ln 2 ms). The full display gray-scale ranges from +1 to −1 and linearly covers a 144 ms difference in T_1. With conventional T_1 maps of the brain and CSF the gray-scale range typically covers 2,000–4,000 ms. Thus, there is much greater display sensitivity to differences in T_1 in the mD with the dSIR image than with conventional T_1 maps. Lesions with T_1 values greater than the maximum in the mD (i.e., greater than 924 ms) "overshoot" and have a mid-gray center (where T_1 values shown on the gray-scale are unreliable) and are surrounded by high signal boundaries. T_1 mapping is only valid in the mD. If the TR is short, the values may be low and need correction. In this case, the source images were obtained using a long TR IR sequence. mD, middle domain; dSIR, divided inversion recovery; TI_s, short TI; TI, inversion time; TI_i, intermediate TI; CSF, cerebrospinal fluid; TR, repetition time; IR, inversion recovery.

insight into the properties of the dSIR T_1-filter. To do this, a linear equation of the form y = mx + c between the end points of the mD can be produced by fitting a straight line between the first and last points of the mD (i.e., first point x = TI_s/ln 2 and y = −1, and last point x = TI_i/ln 2 and y = + 1). It is an approximation to the dSIR T_1-filter in the mD, so S_{dSIR} in the mD is given by:

$$S_{dSIR} \approx \frac{\ln 4}{\Delta TI} T_1 - \frac{\Sigma TI}{\Delta TI} \quad [22]$$

where $\Delta TI = TI_i - TI_s$ (i.e., second longer TI minus first shorter TI which is positive) and $\Sigma TI = TI_s + TI_i$. The convention for ΔTI is to define it by the subtraction: second TI minus first TI so ΔTI is positive for dSIR T_1-bipolar filters and negative for drSIR T_1-bipolar filters. The sign of ΔTI depends on whether the second TI is greater or less than the first TI.

Note that because ΔTI is positive, and the slope $\frac{\ln 4}{\Delta TI}$ in Eq. [22] is positive (e.g., *Figure 9C*) the contrast is positive.

The same approach applies to the drSIR T_1-bipolar filter where the first point is x = TI_i/ln 2 with y = −1, and the second point is x = TI_s/ln 2 with y = 1. S_{drSIR} in the mD is given by:

$$S_{drSIR} \approx \frac{\ln 4}{\Delta TI} T_1 - \frac{\Sigma TI}{\Delta TI} \quad [23]$$

where ΔTI = the second TI, TI_s − the first TI, TI_i which is negative, and $\Sigma TI = TI_s + TI_i$. Since ΔTI is negative, the slope $\frac{\ln 4}{\Delta TI}$ in Eq. [23] is negative (e.g., *Figure 12C*) and the contrast is positive.

The expressions in Eqs. [22,23] capture four key features of the dSIR and drSIR T_1-bipolar filter, firstly, the near linear change in signal with T_1 in the mD, secondly, the T_1-bipolar filters have slopes equal to $\frac{\ln 4}{\Delta TI}$, and thirdly, the T_1-bipolar filter show high contrast sensitivity for small changes in T_1 when the size of ΔTI is small (since $\Delta S_{dSIR} \approx \frac{\ln 4}{\Delta TI} \Delta T_1$ and $\Delta S_{drSIR} \approx \frac{\ln 4}{\Delta TI} \Delta T_1$). As ΔTI decreases in magnitude, amplification of contrast increases (*Table 2*). Fourthly the equations can be used to map T_1 in the mD since for S_{dSIR} and S_{drSIR}:

$$T_1 \approx \frac{\Delta TI}{\ln 4} S_{dSIR} - \frac{\Sigma TI}{\ln 4} \quad [24]$$

$$T_1 \approx \frac{\Delta TI}{\ln 4} S_{drSIR} - \frac{\Sigma TI}{\ln 4} \quad [25]$$

The S_{dSIR} and S_{drSIR} maps typically show high contrast and high spatial resolution (e.g., *Figure 19*).

The linear approximation is only valid in the mD. Also, it is assumed that TR is long otherwise T_1 values may require correction for incomplete recovery of longitudinal magnetization during TR. It is also assumed that the nulling of the baseline tissue is accurate.

GBCA enhancement

The effect of GBCA is to decrease T_1 (i.e., produce a negative ΔT_1) so, in order to see positive contrast enhancement, drSIR sequences are used as shown in *Figures 11,12*.

The baseline tissue may be normal or abnormal. In the latter case, its T_1 may be prolonged and so the initial TI may need to be lengthened to correspond to this and thus be greater than that for normal tissue.

There is interest in both the image contrast produced by the GBCA and the specific effect of the agent itself. The image contrast may be demonstrated by appropriate choice of ΔTI. The specific effect of the agent can be found from the subtraction: post minus pre with the same IR sequence i.e., the baseline nulling sequence.

It is possible to choose several TIs so that image contrast increases can be observed in several tissues simultaneously.

The process of intravenous injection of a GBCA usually displaces the head between pre and post GBCA acquisitions relative to the scanner. 3D isotropic acquisitions with rigid body registration are a preferred way to deal with the resulting misregistration.

The focus is on subtle GBCA contrast enhancement including the types that delayed and double dose contrast agent regimes have been used for. It may also be possible to use lower doses of GBCAs.

Dynamic contrast enhancement and modeling of GBCA distribution may be improved by having greater sensitivity to T_1 shortening produced by smaller quantities of GBCAs early in the enhancement process.

GBCA enhancement may be seen in CSF using the T_2-FLAIR sequence as a baseline, but inflow of CSF during TI may produce shortening of the effective T_1 of CSF and be a confounder. This can be addressed with a thicker slice, or non-slice selective inversion pulses (24).

Serial studies

In general terms, there is no special premium in clinical MRI in demonstrating high contrast lesions with even greater contrast. The emphasis with MASDIR sequences is on demonstrating contrast in situations where there are only small changes in TPs and, as a consequence, little or no contrast is seen with conventional sequences. The emphasis is therefore on imaging regimes which detect small changes in TPs. Ideally these can allow disease to be monitored over time to follow its natural history and the effects of treatment.

Increased sensitization in the mD is produced by a decreased width of the mD and decreased magnitude of ΔTI. This is particularly appropriate for detecting small changes in T_1 from normal to abnormal in specific tissues. These changes may be seen in earlier stages of disease as well as in more subtle forms of disease.

In addition to contrast due to differences or changes in T_1 as above, magnetic resonance (MR) images may show differences in signal (or contrast), due to differences in the spatial properties of tissues e.g., their size, site, shape and surface. This applies to normal and abnormal tissues.

The changes from normal in signal and space seen in a single image may vary over time in serial studies as part of the natural history of the disease and/or the result of therapy. In situations where the changes in signal and/or space are small, rigid body registration can accurately align images obtained on two or more examinations so that genuine changes can be distinguished from artefactual differences due to variation in slice alignment at the different examinations (i.e., misregistration).

This has been performed with 3D isotropic spoiled gradient echo (GE) sequences, and a system of interpreting subtracted images has been described (25). MASDIR sequences using 3D MP-RAGE or brain volume (BRAVO) type data acquisitions with rSIR or drSIR image processing offer increased sensitivity to changes in T_1 compared with spoiled GE sequences. They also offer high signal boundaries to improve detection of changes in the spatial properties of tissues. This option is not available with spoiled GE sequences.

A major advantage with serial studies is that the patient may act as her/his own control with the initial images providing a baseline to recognize small changes in T_1 and/or image spatial properties on subsequent examinations using registration. These might not be recognizable on a single image seen in isolation.

Quantitation

The fact the dSIR and drSIR images can directly provide

values of T_1 in the mD is valuable for quantitation. This can include decrease in T_1 due to GBCA enhancement. In addition, the high signal boundaries are of value in quantifying spatial properties of normal tissues and lesions such as the volume of lesions or parts of them (as well as changes in volumes) in serial studies.

Summary of key concepts affecting the understanding and use of rSIR and drSIR sequences

Targeting

(i) In this work, tMRI is typically aimed at small changes in T_1 and the spatial properties from normal in single tissues;
(ii) The tissues of interest are normal or near normal appearing white or gray matter;
(iii) The changes in T_1 and spatial properties may arise from disease of the brain or other causes (e.g., physiological changes, contrast agents and drugs);
(iv) The normal or near normal appearances of white or gray matter are usually those shown with MP-RAGE, T_2-wSE, and/or T_2-FLAIR sequences;
(v) For small changes in T_1 from normal, narrow mD dSIR and drSIR sequences can usefully produce contrast up to about 15 times greater than that generated by conventional MP-RAGE sequences, and so make the effects of small changes in T_1 visible on dSIR and drSIR images when they are not seen on conventional images;
(vi) The dSIR and drSIR sequences need to be targeted to the T_1 of the normal tissue for nulling as well as the sign and size of the change in T_1 being sought. This is done by appropriate choice of their TIs, i.e., the nulling TI and the difference in TI, ΔTI are matched to the change in T_1, ΔT_1.

Mathematical modeling

(i) The modeling employs TP-filters which are plots of signal against TP or ln TP for segments of sequence or sequences;
(ii) The contrast generated by a small change in a TP is the change in that TP multiplied by the slope of its TP-filter. The overall fractional contrast produced by a sequence is the algebraic sum of the contrasts generated by each TP in that sequence. This is expressed as the CCT. It is derived from the Bloch and Torrey equations using the product rule of differential calculus;
(iii) The single TP T_1 is used 3–4 times to generate synergistic T_1 contrast with the dSIR and drSIR T_1-bipolar filters;
(iv) The T_1-bipolar filters of the dSIR and drSIR sequences are used to describe the targeting, signal, contrast, boundaries, T_1 mapping and GBCA enhancement of the two sequences;
(v) The contrast at boundaries (change in signal ΔS with distance x) is the product of the sequence weighting (slope of the T_1-filter), the change in T_1 with tissue fraction (f) and the change in f with distance x. This follows from the chain rule of differential calculus;
(vi) In the mD of the dSIR and drSIR T_1-bipolar filters, there is a near linear relationship between signal and T_1 so dSIR and drSIR images can be calibrated as T_1 maps in the mD. When the magnitude of the difference in TI (ΔTI) is decreased, contrast amplification is increased until the stage is reached where images become noise and/or artefact limited.

Radiology

(i) Contrast: contrast can be targeted at normal or normal appearing white or gray matter and can be produced where it is particularly needed i.e., for improving visualization of subtle disease where there are only small changes in T_1 from normal, so that contrast is not shown, or only poorly shown, with conventional sequences;
(ii) Boundaries: the dSIR sequence can produce high signal, often high contrast boundaries between white and gray matter, between white matter and CSF, between cortical gray matter and CSF, as well as between normal and abnormal tissues;
(iii) T_1 maps: because of the normalization of signals with dSIR and drSIR images, ρ_m and T_2 effects are largely eliminated so dSIR and drSIR images are essentially T_1 maps. There is a near linear relationship between signal and T_1 in the mD which can provide direct reading of T_1 values in areas of interest;
(iv) GBCA enhancement: the narrow mD drSIR sequence is highly sensitive to reductions in T_1 produced by GBCAs;
(v) Serial studies: using rigid body registration of isotropic 3D images, changes in T_1 can be demonstrated. On

Table 4 Pulse sequences and pulse sequence parameters used at 3T

#	Sequence	TI (ms)	TE (ms)	Matrix and voxel size (mm)	Slice thickness (mm)
1	2D FSE IR (for white matter nulling)	350	7	256×224; Z512; 0.4×0.4	4
2	2D FSE IR (used with #1 for narrow mD dSIR)	500	7	256×224; Z512; 0.4×0.4	4
3	2D FSE IR (used with #1 for intermediate mD dSIR)	650	7	256×224; Z512; 0.4×0.4	4
4	2D FSE IR (used with #1 for wide mD dSIR)	800	7	256×224; Z512; 0.4×0.4	4
5	3D BRAVO with prospective motion correction (PROMO) (for white matter nulling)	350	2.8	240×240; 1×1	1
6	3D BRAVO with prospective motion correction (PROMO) (used with #5 for narrow mD dSIR)	450	2.8	240×240; 1×1	1
7	3D BRAVO with prospective motion correction (PROMO) (used with #5 for intermediate mD dSIR)	650	2.8	240×240; 1×1	1
8	3D BRAVO with prospective motion correction (PROMO) (used with #5 for wide mD dSIR)	750	2.8	240×240; 1×1	1
9	2D T_2-wSE	2,200	102	300×280; Z512; 0.5×0.5	4
10	3D T_2-FLAIR	1,851	102	256×256; Z512; 0.5×0.5	0.8

TI, inversion time; TE, echo time; 2D FSE IR, two-dimensional fast spin echo inversion recovery; Z, zipped; mD, middle domain; dSIR, divided subtracted inversion recovery; 3D BRAVO, three-dimensional brain volume; 2D T_2-wSE, two-dimensional T_2-weighted spin echo; 3D T_2-FLAIR, three dimensional T_2-fluid attenuated inversion recovery.

registered images, the high signal boundaries produced by the dSIR and drSIR sequences can also be used to demonstrate changes in the spatial properties (e.g., size, shape, site, surface) of normal structures and lesions over time in serial MR examinations;

(vi) Quantitation: dSIR and drSIR images provide direct measurement of T_1 in the mD. This can be extended to GBCA enhancement including modeling of its distribution. T_1 measurements can be supplemented by quantitation of spatial features using the high signal boundaries produced by dSIR and drSIR sequences.

Implementation of dSIR and drSIR sequences and their failure modes

Implementation

The source sequences for dSIR and drSIR images are typically conventional two-dimensional (2D) IR fast SE (FSE) and 3D IR GE (e.g., 3D MP-RAGE, BRAVO, or 3D fast field echo) sequences which are available on most clinical MR systems. The TEs are typically short e.g., 5–10 ms for FSE and 1–5 ms for GEs (*Table 4*). Comparable or slightly higher spatial resolution conventional sequences were performed for comparison using the same types of data acquisition.

In targeting the source IR images, the initial task is to select the tissue of primary interest and determine the TI needed to null it (*Figure 20*). The choice of TI may be based on a knowledge of tissue T_1s and nulling TIs, experience with similar cases and recognition of the technical factors which change the nulling TI as well as conditions which change the T_1 of tissues to be nulled [see *Tab. 8* in (23)].

In general, at least initially, it is worth testing to ensure that the tissue of interest is nulled and, if there is doubt, when seeking changes that increase T_1 use a TI slightly less than the expected value. Errors in this direction generally have a benign effect on contrast.

The next decision is the expected sign of the change in T_1 i.e., positive or negative. This determines whether the second TI used is higher (increase in T_1) or lower (decrease in T_1 than the nulling TI. After this, a decision needs to be made on the magnitude of the difference in TI i.e., ΔTI. Smaller TIs give higher amplification of contrast but if the change in T_1 takes it outside the mD this results in overshoot. ΔTI determines the width of the mD which may be narrow, intermediate or wide. For white matter, using a dSIR sequence and seeking an increase in T_1 with a longer second TI, a narrow ΔTI is about 20% to 40%, an intermediate ΔTI is about 40% to 60%, and a wide ΔTI is

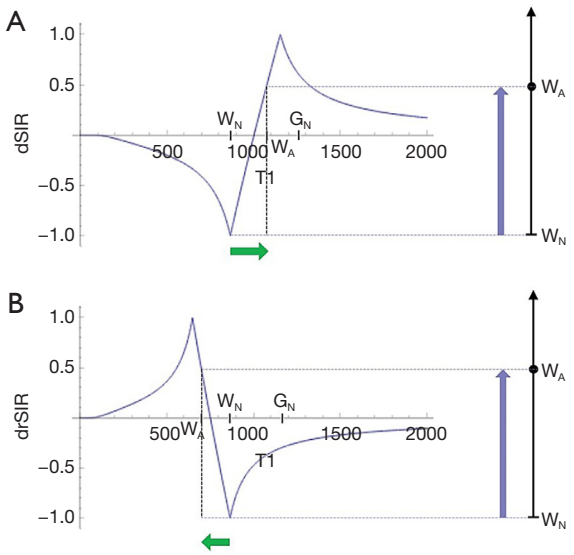

Figure 20 Targeting of dSIR (A) and drSIR (B) T_1-bipolar filters for small changes in T_1 from normal. T_1 is shown along the X axis in ms. In (A) the dSIR T_1-bipolar filter nulls normal white matter with a T_1 W_N using the first TI, and is targeted for the location and the size of the mD using the second longer TI for a small increase in the normal white matter T_1 from W_N to W_A (positive horizontal green arrow). ΔTI is positive. This produces positive contrast (blue arrow on right). In (B) the drSIR T_1-bipolar filter nulls normal white matter with T_1 W_N using the first TI. The location and size of the mD is targeted for a small decrease in the white matter T_1 from W_N to W_A (negative horizontal green arrow) using the second shorter TI. ΔTI is negative. This produces positive contrast (blue arrow on right). dSIR, divided subtracted inversion recovery, W_N, white normal; G_N, gray normal; W_A, white abnormal; drSIR, divided reverse subtracted inversion recovery; TI, inversion time; mD, middle domain.

about 80% or more. The objective is to match the position and size of the mD to the position, sign and size of the change in T_1 so that the sequence is correctly targeted.

When targeting white matter, the choice of narrow, intermediate or wide mD also determines the location of high signal boundaries. If the second TI is less than that needed to null cortical gray matter, the high signal boundary will be within the brain between white matter and cortical gray matter. If the second TI is greater than that needed to null cortical gray matter the boundary will be outside of the brain at the junction between cortical gray matter and CSF.

For other tissues the location and width of the high signal boundaries follows from the same considerations as in *Figures 14,17*. Narrow boundaries are found with small magnitudes of ΔTI and narrow mDs. Wider boundaries are found with larger magnitudes of ΔTI and wider mDs.

The image processing uses the images acquired with the two different TIs, and does the subtraction: shorter TI image minus longer TI image to give SIR images and the reverse subtraction: longer TI image minus shorter TI image to give rSIR images. The two original images are then added to give an AIR image which is used in the denominator to divide the SIR and rSIR images to give dSIR and drSIR images respectively. This is performed for both 2D and 3D images.

For GBCA enhancement there is usually displacement of the patient's head between pre and post contrast images relative to the MR system, so 3D isotropic GE acquisitions are used, and rigid body registration is used to align the pre and post images and allow subtraction without misregistration. drSIR sequences are used and the initial nulling TI for contrast enhancement may need to be prolonged if a lesion with an increased T_1 is being studied, or shortened if a lesion with a decreased T_1 is being studied (*Figure 21*). Subtractions performed after GBCA administration may be targeted at (i) image contrast and (ii) specific effects of the GBCA.

In serial studies performed at different times, in addition to changes in signal and contrast there may be changes in space (e.g., change in site, shape, size and surface of normal tissues or lesions as with growth or regression of a tumor). If the changes are relatively small, rigid body registration can also be used to precisely align images obtained at different times. This is often the situation with dSIR and drSIR images when they are used for detection of small changes in T_1 and/or spatial properties. If changes are large, non-rigid body registration may be needed. This is less precise than rigid registration, but if the changes are large, image interpretation is usually straightforward.

Failure modes

Failure modes need to be recognized, preferably at an early stage so the rest of the examination is not compromised.

(i) The commonest problem is failure to null the normal tissue of primary interest. Usually, the TI is too long and this reduces the contrast produced on dSIR images when nulling white matter and seeking an increase in T_1 in disease. The precise value of TI for nulling can vary for technical reasons e.g., with field strength, the value of TR, the recovery time, the efficiency of the B_1 pulse,

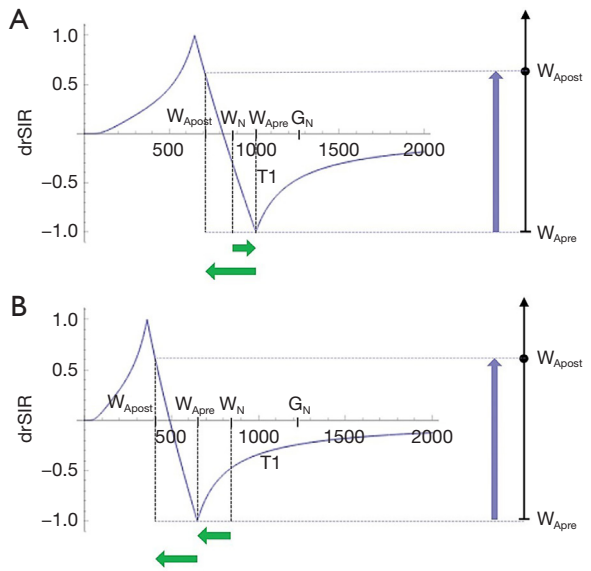

Figure 21 Targeting of drSIR T_1-bipolar filters for GBCA enhancement in lesions with an increase in T_1 (A) and a decrease in T_1 (B). T_1 is shown along the X axis in ms. In (A) the lesion in white matter has increased its T_1 from W_N to W_{Apre} (upper positive horizontal green arrow). The drSIR T_1-bipolar filter is targeted at a decrease in T_1 due to GBCA enhancement from W_{Apre} to W_{Apost} (lower negative horizontal green arrow). ΔTI is negative. This produces positive contrast (vertical blue arrow on right). In (B) the lesion in white matter has decreased its T_1 from W_N to W_{Apre} (upper negative horizontal green arrow). The drSIR T_1-bipolar filter is matched for a further decrease in T_1 with GBCA enhancement from W_{Apre} to W_{Apost} (lower negative horizontal green arrow). ΔTI is negative. This produces positive contrast (vertical blue arrow on right). Thus, tMRI for GBCA enhancement may require the use of additional longer and shorter TIs to bracket the expected reduction in T_1. drSIR, divided reverse subtracted inversion recovery; W_{Apost}, white abnormal post-enhancement; W_N, white normal; W_{Apre}, white abnormal pre-enhancement; G_N, gray normal; GBCA, Gadolinium based contrast agent; tMRI, targeted magnetic resonance imaging; TI, inversion time.

B_1 homogeneity, data collection (GE *vs.* FSE) use of fast recovery and fat saturation. The T_1 of the tissue to be nulled can vary with subject age, location in the brain etc. Cancellation lines are seen at the boundary between two tissues on magnitude images when the longitudinal magnetization of one tissue is positive and the other is negative. They occur when white matter is being nulled if the TI being tested for nulling is too long so that the 90° pulse and sampling is too late. The white matter longitudinal magnetization (M_z) is then positive (not zero as it would have been if the white matter had been nulled) and gray matter M_z is negative. If the TI is too short, both the white and gray matter have negative M_zs. As a result, there is signal on magnitude images, but no cancellation line between the two tissues;

(ii) It is also possible to choose the wrong sign for the change in T_1 in disease e.g., be set up for an increase in T_1 and the disease produces a decrease in T_1;

(iii) The mD may be too narrow leading to signals which overshoot the mD of the dSIR or drSIR sequences. This occurs when the changes in T_1 are greater than expected. With dSIR sequences set up for an increase in T_1, it typically results in a high signal around the lesion with intermediate signal inside the boundary;

(iv) The mD may be too wide leading to low contrast for the change in T_1;

(v) The boundary location and width may be inappropriate. If the first TI is chosen to null white matter, and the second TI is chosen to null gray matter, the boundary between the two may be isointense with gray matter and so may not be apparent;

(vi) Misregistration is usually obvious, with for example high and low signals at lateral ventricular boundaries. Correction of misregistration with 2D images may be possible to a reasonable degree with shifting of the second image by a few voxels and/or fractions of a voxel. Rigid body registration of isotropic 3D images is usually a more satisfactory solution;

(vii) Partial volume effects from high signal boundaries may simulate lesions particularly with 2D acquisitions using a thick slice e.g., 3–4 mm compared with the typical 1 mm slice thickness of 3D acquisitions;

(viii) Errors in T_1 may arise from:
- (a) inaccurate tissue nulling;
- (b) use of a short TR;
- (c) measurement outside of the mD;

(ix) It may be useful to label accurate T_1 values in the mD on images by color, or use a mask to separate them from inaccurate T_1 values outside of the mD;

(x) The MP-RAGE sequence has limitations on the TI needed to achieve white matter nulling

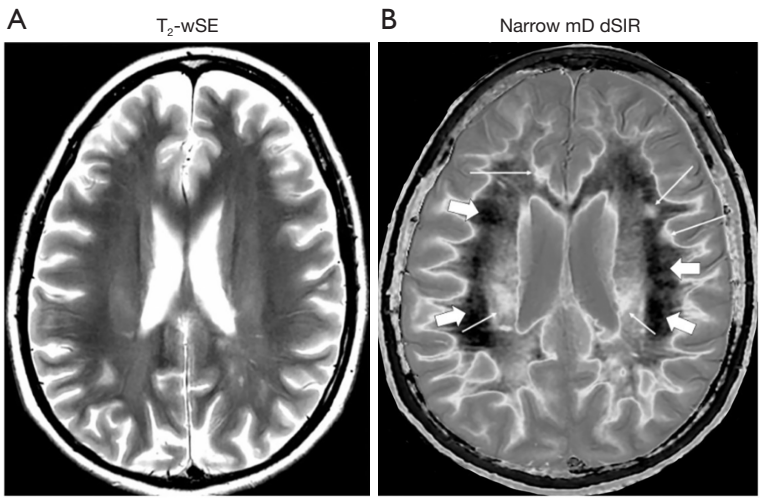

Figure 22 Case of MS. Comparison of 2D T_2-wSE (A) and narrow mD dSIR (B) images using similar spatial resolutions and slice thicknesses. The narrow mD dSIR sequence is targeted to null normal white matter and produce high positive contrast from small increases in T_1 from the normal T_1 of white matter. No abnormality is seen on the T_2-wSE image but three focal lesions are seen on the dSIR image (long thin arrows). The corticospinal tracts are also abnormal (short thin arrows). The normal superior longitudinal fasciculi are of intermediate signal in (B). More peripheral white matter appears dark and much of it is normal in (B) (thick arrows). Thus, the lateral peripheral normal appearing white matter in (A) is mostly normal in (B). A high signal boundary is seen between white matter and cortical gray matter as well as at the white matter-CSF boundary around the lateral ventricles. T_2-wSE, T_2-weighted spin echo; mD, middle domain; dSIR, divided subtracted inversion recovery; MS, multiple sclerosis; 2D, two-dimensional, CSF, cerebrospinal fluid.

imposed by the minimum TR which are not found with the BRAVO sequence. Increasing the TR may resolve the problem by making shorter TIs accessible.

Examples

Application of these principles can be seen in a case of MS (*Figure 22*) which compares a T_2-wSE image (*Figure 22A*) with a narrow mD dSIR image (*Figure 22B*). This image (*Figure 22B*) is targeted to null normal white matter and produce high positive contrast from small increases in white matter T_1 from normal. No abnormality is seen in (*Figure 22A*) but three focal lesions are seen in (*Figure 22B*) (long thin arrows). One is in white matter; another is at the junction between white and gray matter (anterior); and the other is at the junction between white and gray matter but mostly in gray matter (left). Localization of lesions is helped by the well defined high signal white matter gray matter boundaries. High signal is seen in the corticospinal tracts (short thin arrows). Normal white matter is seen laterally and has a low signal (dark) appearance in (*Figure 22B*) (thick arrows). Intermediate signal is seen in the more medial normal superior longitudinal fasciculi in (*Figure 22B*).

Figure 23 is a higher slice in the same case as in *Figure 22* where a T_2-wSE image is compared with a narrow mD dSIR image. No abnormality is seen on the T_2-wSE image (*Figure 23A*) but a focal lesion is seen on the dSIR image (long thin arrow) (*Figure 23B*). The corticospinal tracts are also seen (short thin arrows). There are areas of increased signal in most of the white matter in (*Figure 23B*) (thick arrows). Only about 5–10% of the white matter has a low signal (dark) and appears normal. High signal boundaries are seen between white and gray matter.

In *Figure 22* most of the normal appearing white matter on the T_2-wSE image (*Figure 22A*) shows as normal tissue with a dark (low) signal appearance in *Figure 22B* (thick arrows). In *Figure 23*, most of the normal appearing white matter in *Figure 23A* shows abnormal high signal in *Figure 23B* (thick arrows). Even in retrospect it is not possible to decide whether the normal appearing white matter in *Figures 22A*,*23B* will appear normal or abnormal on the corresponding narrow mD dSIR images.

In another case of MS, no abnormality is seen on the T_2-FLAIR image (*Figure 24A*) in the thalamus, but a focal lesion

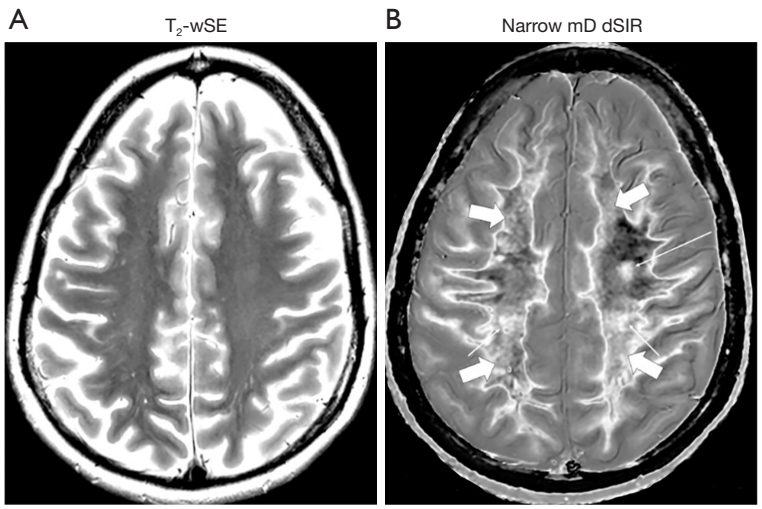

Figure 23 Same case of MS as in *Figure 22* shown at a higher level. Comparison of T_2-wSE (A) and narrow mD dSIR (B) images. The narrow mD dSIR sequence is targeted to null normal white matter and produce high positive contrast from small increases in T_1 from the normal T_1 in white matter. A focal lesion that is not seen on the T_2-wSE image is seen on the dSIR image (long thin arrow) and other abnormalities are seen in the corticospinal tracts (short thin arrows). The white matter appears normal on the T_2-wSE image (A) but most of it has a high signal and appears abnormal on the narrow mD dSIR image (B) (thick arrows). Only about 5–10% of the white matter in (B) has a normal dark appearance. The normal appearing white matter in (A) mostly appears abnormal in (B). High signal boundaries are seen between white matter and cortical gray matter. T_2-wSE, T_2-weighted spin echo; mD, middle domain; dSIR, divided subtracted inversion recovery; MS, multiple sclerosis; CSF, cerebrospinal fluid.

is seen in the thalamus using an intermediate mD dSIR sequence (thin white arrow) (*Figure 24B*). The intermediate mD dSIR sequence is targeted to null white matter and produce positive contrast from increases in T_1 over a broader domain than in *Figures 22B,23B*. *Figure 24B* which used an intermediate mD shows less lesion contrast in white matter than *Figures 22B,23B* which used narrow mDs.

Figure 25 shows narrow mD dSIR images in a normal, gender, ethnicity and socio-economically matched 49-year-old control (left column), and a 51-year-old patient with methamphetamine dependency for 20 years followed by an abstinence period of 120 days (right column). In the control images, most white matter appears normal with a low signal (dark) (left column), but in the patient most white matter appears abnormal with a high signal (light) (right column). There is only a small amount of normal white matter (dark) present on the patient's images (thin white arrows, right column).

In the normal control, there is contrast between more peripheral normal white matter (dark) (left column) and more central normal white matter of the superior longitudinal fasciculi (mid-gray).

Figure 26 compares a T_2-FLAIR image (*Figure 26A*) with a narrow mD dSIR image (*Figure 26B*) in the 51-year-old patient. No abnormality is seen on the T_2-FLAIR image (i.e., it shows normal appearing white matter) but extensive high signal abnormalities are seen in white matter on the narrow mD dSIR image. There are only small areas of normal low signal (dark) white matter on this image (thin arrows).

Figure 27 shows comparison of 3D T_2-FLAIR images (left column) and 3D intermediate mD dSIR images (right column) in another patient with methamphetamine dependency. Focal lesions are seen in white matter on both the T_2-FLAIR and intermediate mD dSIR images (thin arrows). The intermediate mD dSIR images are less sensitive to change in white matter than the narrow mD dSIR images shown in *Figure 25* (right column) and *Figure 26B*. The comparison illustrates the benefits of using a narrow mD to achieve high lesion contrast compared with using an intermediate mD where the lesion contrast is lower and about the same as that seen on the T_2-FLAIR image.

Discussion

The use of dSIR and drSIR sequences described in this

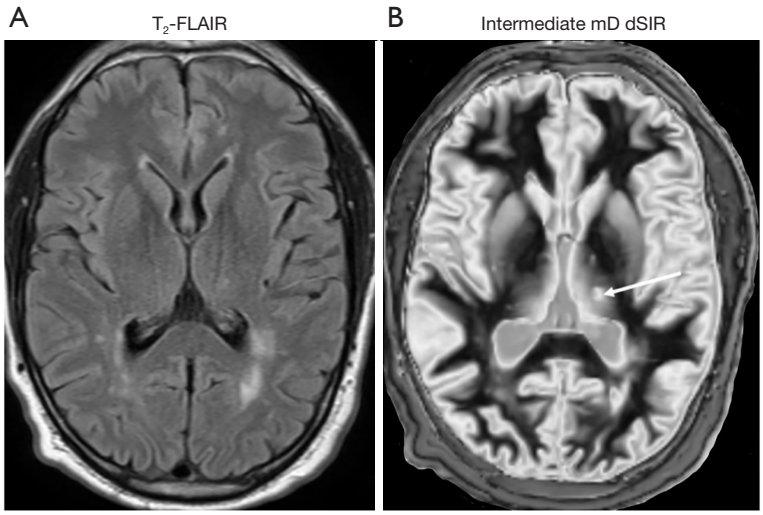

Figure 24 Case of MS examined at 1.5T. T_2-FLAIR (A) and intermediate mD dSIR (B) images. White matter is nulled and the sequence is sensitive to increases in T_1 over an intermediate T_1 domain. The boundary line between white matter and gray matter is isointense with gray matter. A lesion is seen in the left thalamus in (B) (long thin arrow) but not seen on the T_2-FLAIR image (A). White matter lesions are much less obvious on the intermediate mD image (B) than on the narrow mD images shown in previous *Figures 22B*,*23B*. T_2-FLAIR, T_2-fluid attenuated inversion recovery; mD, middle domain; dSIR, divided subtracted inversion recovery; MS, multiple sclerosis.

paper follows directly from the CCT. Increased sequence weighting (higher slope of the T_1-bipolar filter in the mD) is used to compensate for the small change in T_1 (ΔT_1) which may be present in normal appearing tissues but be insufficient to produce contrast with the lower slope T_1-bipolar filters of conventional sequences. The region of the T_1-bipolar filter which has the steepest slope is the mD, and this needs to be narrow for high contrast amplification. This is not a problem when the objective is to image small changes in T_1 which can easily be accommodated within a narrow mD. Detection of small changes in T_1 in normal appearing tissues is therefore a very appropriate application for targeted narrow mD dSIR and drSIR sequences.

Targeting

All MRI examination are targeted to a lesser or greater extent. Even whole-body MRI includes sequences sensitive to only a few TPs (*Table 5*). The term tMRI is usually applied to sequences focused on specific tissues, their TPs and changes in these TPs in disease (e.g., #4–7 in *Table 5*). This is greater targeting than that of typical conventional T_1-wSE and IR sequences in which there is sensitivity to changes in T_1 over a relatively broad T_1 domain as shown by the slopes of their filters. They typically have a maximum slope centrally but lesser slopes extending out on either side to flat plateaus at low and high values of T_1 where there is less sensitivity to changes in T_1 (*Figures 3*,*6*). Narrow mD dSIR and drSIR sequences are highly sensitive to small changes in T_1 in the mD (*Figures 9*,*11*). dSIR and drSIR sequences are generally less sensitive to changes in T_1 outside of the mD. Larger changes in T_1 in the domains outside of the mD can usually be shown with conventional sequences.

dSIR and drSIR T_1-bipolar filters

The dSIR and drSIR T_1-bipolar filters provide keys to understanding the targeting, signal, contrast, boundaries, T_1 mapping and GBCA enhancement seen on the dSIR and drSIR images. dSIR and drSIR T_1-bipolar filters are univariate for T_1 (i.e., dependent on T_1 but not on ρ_m or T_2) and are comprehensive i.e., only a T_1 TP-filter is needed to interpret dSIR and drSIR images unlike, for example, SE and T_2-FLAIR images where three different TP-filters (ρ_m, T_1, and T_2) are needed to understand them.

As the magnitude of ΔTI and the matched change in T_1 ΔT_1 become smaller, the small change approximation of differential calculus used in the CCT, and the linear approximation used for T_1 mapping both become more accurate. Ultimately, however, the images become signal

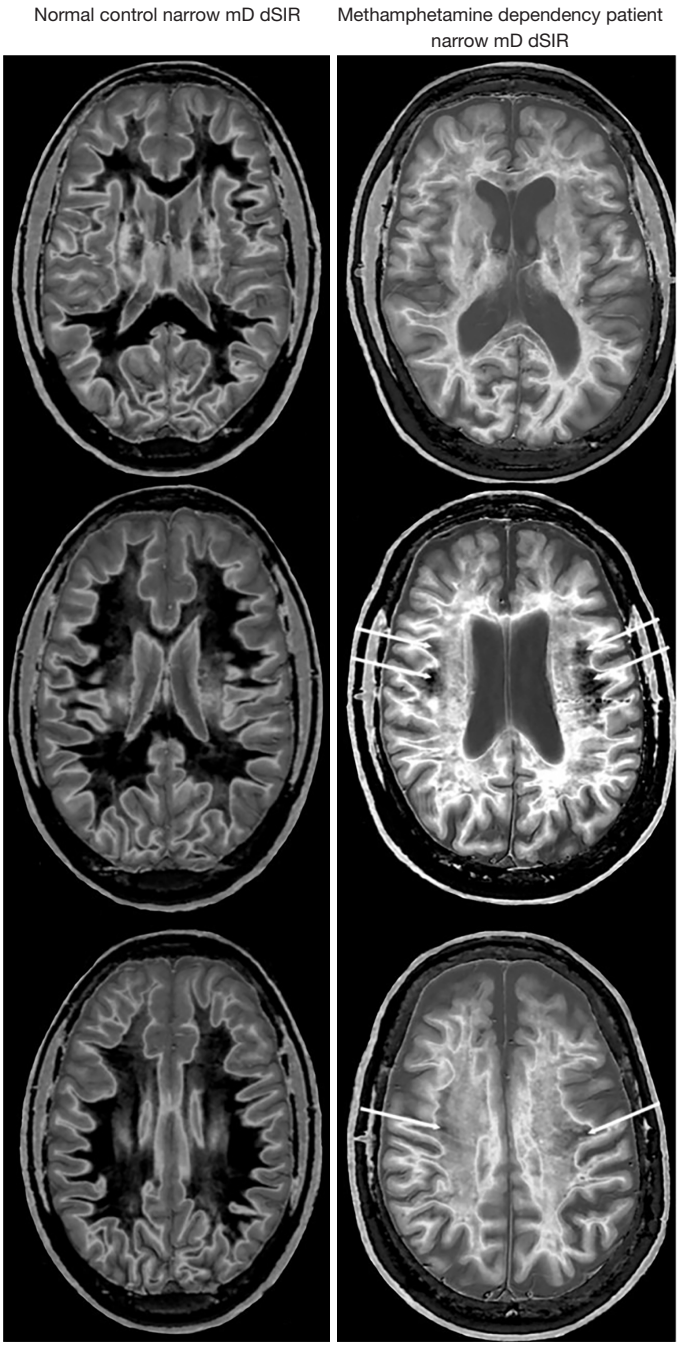

Figure 25 This shows 2D narrow mD dSIR images in the gender, ethnicity, and socioeconomic status matched 49-year-old normal control (left column) and in the 51-year-old male with a 20-year history of methamphetamine dependency, abstinence period 120 days (right column). The narrow mD sequences are targeted to null normal white matter and highlight contrast produced by small increases in the T_1 of normal white matter. The narrow mD dSIR images in the control show normal white matter as low signal (dark). The dSIR images in the methamphetamine patient (right column) show widespread high signal (light) in white matter with only small areas of normal dark white matter (long thin arrows). Normal high signal boundaries are seen between white matter and gray matter in both sets of dSIR images but are more obvious in the normal control. They are partly obscured by the abnormal high signal in white matter in the patient. Contrast is seen between some normal central white matter in superior longitudinal fasciculi (light) in the normal control and more peripheral normal white matter (dark) (left column). mD, middle domain; dSIR, divided subtracted inversion recovery; 2D, two-dimensional.

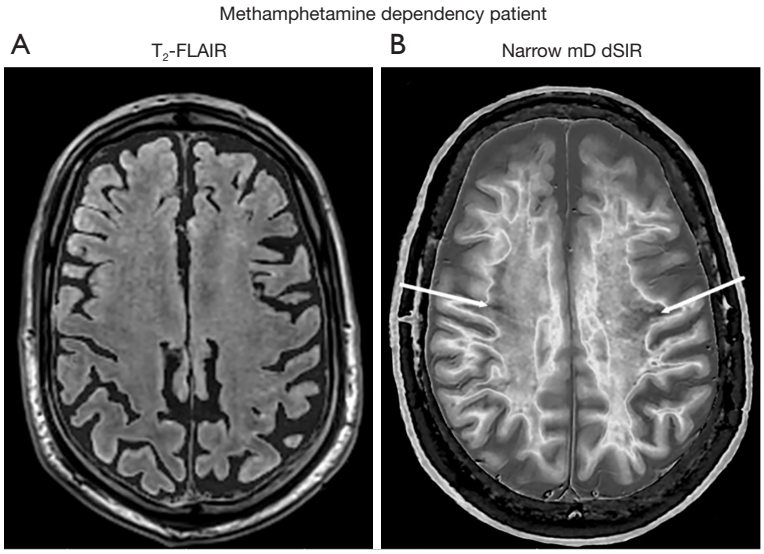

Figure 26 Methamphetamine dependency patient. Comparison of 2D T_2-FLAIR (A) and narrow mD dSIR (B) images with similar spatial resolutions in the 51-year-old patient with a 20-year history of methamphetamine dependency whose images are shown in *Figure 25*. There is normal appearing white matter on the T_2-FLAIR image (A) but on the narrow mD dSIR image (B) there are extensive areas of higher signal in about 90% of the white matter of the centrum semiovale. Only small areas of more normal lower signal are seen in this white matter (long thin arrows) (B). Thus, most of the normal appearing white matter in (A) appears abnormal in (B). High signal boundaries are seen between white matter and gray matter on the narrow mD dSIR image (B). T_2-FLAIR, T_2-fluid attenuated inversion recovery; mD, middle Domain; dSIR, divided subtracted inversion recovery; 2D, two-dimensional.

and/or contrast limited. In addition, as the changes between serial examinations become smaller, rigid body registration becomes more accurate.

Normal tissues

The normal tissues and fluids of primary interest are white matter, cortical gray matter, central gray matter and CSF. Normal white matter may be subdivided into 20 or more categories (26), and cortical gray matter into 4–6 categories. Central gray matter includes many nuclei with varying degrees of organic iron associated with them. The iron shortens T_1 and T_2 but to a first approximation, only the T_1 shortening is relevant with dSIR and drSIR sequences.

It is very helpful to know the T_1s of normal tissues. Since dSIR and drSIR images are T_1 maps and their signals in the mD can be linearly scaled to be T_1 values. The order of tissue signal or brightness directly follows from their T_1 values. Even if the nulling TI is not exact, the order of tissues in the mD (apart from those near the null point) is usually well preserved. Nulling of white matter can be targeted at the shortest T_1 of the relevant normal white matter tissues.

Identification of normal white matter is based on anatomical location, signal in relation to other normal white matter, symmetry, and studies of normal subjects of the same age with the same technique.

The cortex may be more easily visualized with the drSIR sequence for increases in T_1. This makes the boundary between cortex and CSF low signal. Increases in T_1 produce negative contrast in this situation.

Normal appearing tissues

The usual approach to imaging normal appearing tissues such as white and gray matter seen with T_1- and T_2-weighted conventional sequences is to use TPs other than T_1 and T_2 such as magnetization transfer and diffusion, or metabolites using MR spectroscopy. In this paper, the approach to imaging normal appearing white and gray matter is different. A TP (T_1) used with conventional sequences is employed. Small changes in T_1 not seen using conventional T_1-weighted IR sequences are then targeted with dSIR and drSIR sequences.

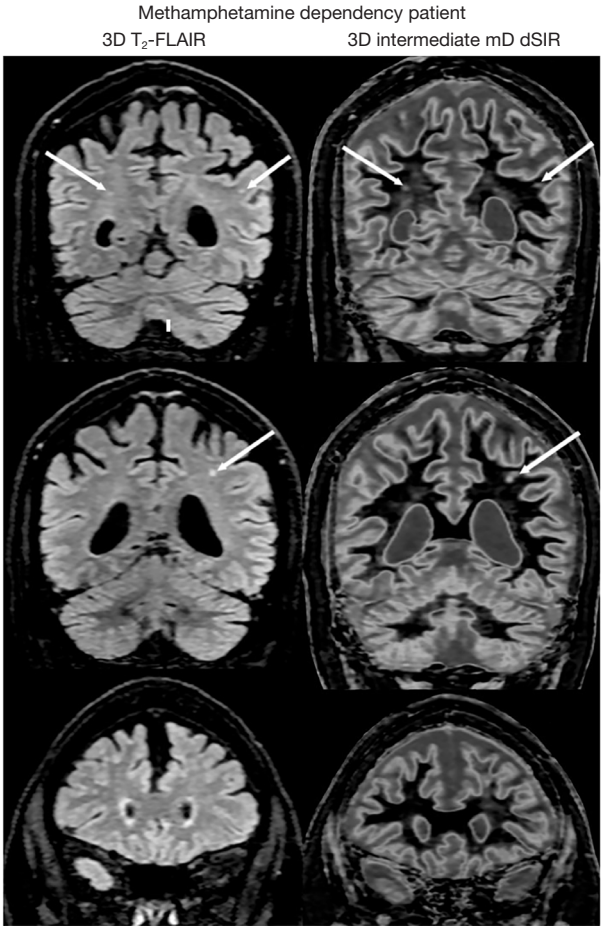

Figure 27 Coronal 3D T_2-FLAIR (left column) and 3D intermediate mD dSIR (right column) images with similar spatial resolutions and slice thicknesses in a 50-year-old male with a 25-year history of methamphetamine dependency and an abstinence period of 80 days. The T_2-FLAIR and intermediate mD dSIR images show similar changes in the white matter (white arrows). The sensitivity of the intermediate mD dSIR images to change in white matter is much less than that of the narrow mD dSIR images shown in *Figures 25*,*26*. T_2-FLAIR, T_2-fluid attenuated inversion recovery; mD, middle domain; dSIR, divided subtracted inversion recovery; 3D, three-dimensional.

Contrast

The most prominent feature of dSIR and drSIR images is their high soft tissue contrast. This may be much greater than that seen with conventional highly T_1-weighted IR sequences such as MP-RAGE. White matter nulled IR sequences of this type are often used to maximize contrast as in the determining anatomy in the thalamus (27), but much higher contrast is available with dSIR and drSIR sequences.

Table 5 Levels of targeting of MRI examinations

#	Target
1	Whole body
2	Region e.g., head, thorax
3	Organ or physiological system e.g., brain, CNS
4	Tissue or tissue components e.g., white matter, myelin water, short T_2 components
5	Tissue or tissue component property e.g., T_1, T_2
6	Sign of change in tissue property
7	Size of change in tissue property

MRI, magnetic resonance imaging; CNS, central nervous system.

Boundaries

The high signal, often high contrast boundaries of dSIR and drSIR are a characteristic feature of these images. Boundary creation of this type can, in principle, be applied to any pair of tissues with different T_1s, subject to noise and/or artefact limitations when the difference in T_1 between the tissue is small and the magnitude of the corresponding ΔTI is small. The objective is to obtain maximum signal from a partial volume affected voxel with a T_1 between those of the two tissues of interest. The approach can be applied to normal tissues to define anatomy, and to normal and abnormal tissues to define lesion boundaries. The sharply defined boundaries of the dSIR and drSIR inages may create the impression that they are of higher spatial resolution than comparable T_2-wSE and T_2-FLAIR images.

dSIR and drSIR images as T_1 maps

Within the mD it is possible to use a linear approximation to produce T_1 maps. The function becomes more linear as the ΔTI and mD are reduced (see *Figure 14A* with a narrow mD and compared with *Figure 14B* with a wide mD).

In comparison with conventional multi-TI T_1 mapping, dSIR and drSIR images/T_1 maps:

(i) require no additional acquisition;
(ii) are usually higher spatial resolution than the multiple TI acquisitions used with conventional T_1 mapping;
(iii) are targeted at the T_1s of interest in the mD rather

than the whole range of T_1s seen on the image and have a narrower range of maximum and minimum values. Rather than values for very long T_1 CSF and short T_1 tissues providing the upper and lower limits of the display gray-scale range as with conventional T_1 maps, dSIR and drSIR images use the same gray-scale for a smaller range of T_1 values and so have higher contrast resolution (i.e., change in the gray scale for the same change in T_1);

(iv) may have reduced partial volume effects because of attenuation of signals towards zero in tissues and fluids outside the mD;

(v) utilize the analytic solutions in Eqs. [24,25]. These provide an alternative to the fitting procedures used in conventional T_1 mapping.

GBCA enhancement

(i) GBCA enhancement may be seen in normal tissue (e.g., white matter) where the initial TI is the same for other studies as well as in abnormal tissues (typically with an increase in T_1) where the initial nulling TI needs to be increased so that the lesion is nulled pre-enhancement and positive contrast can be seen with the reduction in T_1 post contrast using a drSIR sequence;

(ii) The blood brain barrier plays a critical role in disease detection where disruption results in increased GBCA concentration;

(iii) 3D isotropic acquisition with rigid body registration is usually necessary to obtain subtracted images that are not artefacted because of the different locations of pre and post images in the subject;

(iv) Post minus pre GBCA subtractions can be targeted at (a) enhanced lesion contrast by using different TIs, and (b) specific identification of GBCA effects using the same TI;

(v) Quantitation of T_1 change on drSIR images can be directly related to GBCA concentration.

Serial studies

The situations that arise in serial examinations include those seen with tumors and other lesions where there may be changes in T_1 but also changes in site, size, shape, surface etc. which is manifest as differences at lesion boundaries.

The primary interest with dSIR and drSIR images is not in large changes between examinations, which are usually obvious with conventional sequences, but small changes in T_1 and/or the spatial features of tissues. In this situation, rigid body registration may allow accurate registration and recognition of boundaries.

Changes in T_1 may affect the location of boundaries without change in space. Detailed studies may be necessary to determine whether or not this is a significant confounding factor, and how to deal with it.

Quantitation

This exploits the direct measurement of T_1 and the high contrast boundaries produced by dSIR and drSIR sequences. Radiomics and artificial intelligence may benefit from the clarity and analytic form of dSIR and drSIR images.

Cancellation lines

With magnitude reconstructed IR sequences, cancellation lines arise in voxels with mixed tissues where the positive M_z from shorter T_1 tissues is balanced by the negative M_z from longer T_1 tissues so there is no net M_z and therefore no signal after the 90° pulse. Within the brain, when nulling white matter, there is no shorter T_1 tissue present with a positive M_z and so all tissues and fluids including gray matter and CSF have zero or negative M_zs and there is no cancellation line. When using a TI longer than that needed to null white matter, but shorter than that needed to null gray matter, there are voxels with mixtures of white matter (positive M_z) and gray matter (negative M_z). When the proportions balance in mixed tissue voxels there is no net M_z and a cancellation line arises at the boundary between white and gray matter. As TI is increased this occurs up until the TI necessary to null gray matter after which, with further increases in TI, both white and gray matter have positive M_zs. However, voxels with a mixture of white or gray matter and CSF may show positive M_z for one or both of these tissues, and negative M_z for CSF, leading to net zero M_z in voxels at the boundaries between them and CSF so cancellation lines occur at the junction between white or gray matter and CSF.

The subtraction: TI_s image (nulling white matter) minus TI_i image (nulling a T_1 between white and gray matter), and subsequent division with the dSIR image has the cancellation line with zero signal (0) on the longer TI image turned into a high signal (+1) boundary between white and cortical gray matter in voxels with a mixture of white and cortical gray matter just inside cortical gray matter (e.g., *Figure 15*).

The subtraction: TI_s image (nulling white matter) minus

long TI image (nulling a T_1 between those of cortical gray matter and CSF) and subsequent division with the dSIR sequence leads to the cancellation line between cortical gray matter and CSF on the longer TI image becoming a high signal boundary in voxels with a mixture of cortical gray matter and CSF just outside the brain (e.g., *Figure 16*).

This also applies to lesions which have longer T_1s than the nulling T_1 of the second TI sequence. This results in high signal boundaries between normal and abnormal tissue around the lesion with a lower signal within this boundary inside the lesion.

The same general approach applies to the dSIR sequence. The section on contrast at tissue boundaries in this paper provides the mathematical formalism for understanding the contributions to contrast in this situation using T_1-filters, changes in tissue f with T_1 and changes in f with distance (x).

Technical features

(i) The sequences used to create dSIR and drSIR images (2D IR FSE and 3D IR GE) are widely available on standard MRI systems and usually require no special implementation. The sequences require adjustment of their TIs to correspond to the increases in tissues T_1s with increasing B_0. The coding required to add, subtract and divide IR images can written in MATLAB or other similar packages. Rigid body registration packages are widely available e.g., in FSL (fMRIB software library);
(ii) dSIR and drSIR sequences can benefit from interleaving the two different TI acquisitions in a single sequence;
(iii) There are also likely to be benefits in scan time from the use of sense, compressed sense and artificial intelligence;
(iv) Ultra low field imaging e.g., at 0.064T may be feasible with adaption to the short T_1s of white matter and gray matter (275 and 330 ms, respectively, in adults) (28);
(v) Denoising either independently or combined with deep learning may be a significant benefit.

Synthetic dSIR and drSIR images

From Eq. [14] and *Figures 9,12*, it is possible to calculate synthetic dSIR and drSIR images from T_1 maps produced from other sources such as MP2RAGE, MR fingerprinting and actual flip angle-ultrashort TE (UTE) (29). These provide flexibility for targeting and generating contrast using different TIs.

It is also possible to make narrower mD synthetic dSIR and drSIR images from wider mD dSIR and drSIR images. This can provide a series of progressively smaller magnitude ΔTI images to optimize contrast for different ΔT_1s within the mD of the wider dSIR or drSIR image.

Comparison with other sequences

The DIR sequence has partially opposed but net positive T_1-weighting as well as positive T_2-weighting so that for increases in T_1 and T_2 positive synergistic contrast results.

Clinical comparisons of dSIR and drSIR sequences are usually made with MP-RAGE, T_2-wSE (both with a single use of T_2) and/or T_2-FLAIR sequences. The latter has opposed T_1 and T_2 contrast but with increased T_2-weighting due to the use of a longer TE than the conventional T_2-wSE sequences. As a general rule, non-synergistic (e.g., single use of a TP) and opposed contrast sequences do not show contrast due to small changes in T_1 in lesions as well as specifically targeted highly synergistic sequences such as narrow mD dSIR and drSIR sequences.

The FLAWS (18,19) sequence began as separate white matter nulled and CSF nulled IR images. Later developments included division by a single image as the FLAWS division (FLAWS-div) sequence, and division of two subtracted images by the sum of them as the FLAWS-hc and FLAWS-hco images. They are similar to dSIR and drSIR sequences but use wide mDs and are sensitive to changes in T_1 over a broad T_1 domain. They also use two fixed widely spaced TIs. Unlike narrow mD dSIR and drSIR sequences, they are not targeted at small changes in T_1 in specific tissues. The wide mDs of the FLAWS-hc and FLAWS-hco sequences mean that they generally show lower contrast than that seen in the mD of narrow mD dSIR and drSIR sequences. The FLAWS-hc and FLAWS-hco sequences do not have T_1-bipolar filters. Their T_1-filters are essentially monotonic (*Figure 1*) (19). Also, they do not show high signal white matter gray matter boundaries as seen with narrow and intermediate mD dSIR and drSIR sequences.

Tissue targets

Emphasis has been placed on normal white or gray matter as the baseline, reference or nulled tissue. Within gray matter there are specific targets of importance including cortical gray matter and central gray matter nuclei. There are also mixed white and gray matter structures such as the hippocampus, thalamus, brainstem and striate cortex. The T_1 values of central gray matter tissues extend from shorter than white matter for the globus pallidus to about that of

cortical gray matter. It is possible to use a wide mD to cover all gray matter to ascertain T_1s for nulling purposes. It is then possible to focus on specific targets within central gray matter using specific nulling TIs. Disease of central gray matter can result in increases or decreases in T_1.

The complex anatomy and small size of some gray matter nuclei and mixed white and gray matter structures favor the use of thin slice isotropic 3D acquisitions.

In terms of disease, the emphasis to date has been on white matter diseases such as MS which is generally regarded as a neuroinflammatory disease. It could include other diseases which have components of neuroinflammation [in addition to methamphetamine toxicity (30)], such as traumatic brain injury, Alzheimer's disease and Parkinson's disease. Myalgic encephalitis/chronic fatigue syndrome and long coronavirus disease (COVID) are other possibilities. Diffuse relatively low grade neuroinflammation may produce relatively subtle changes in T_1 that only become apparent with dSIR and drSIR sequences.

The increased sensitivity to small T_1 changes, may also help to disentangle demyelination and remyelination processes which often coexist within chronic MS lesions (31).

Different types of white matter disease may be studied, as well as diffusely abnormal white matter (DAWM) seen with conventional sequences (32). The focus could also include cortical gray matter diseases such as focal cortical dysplasia in the workup of epilepsy, as well as discrete cortical demyelinating plaques in MS and other neuroinflammatory diseases.

The high signal white matter gray matter boundaries seen with narrow mD dSIR sequences should allow better characterization of subtle patterns of vasogenic edema associated with neuroinflammatory, neurodegenerative and metabolic conditions. The boundaries may serve as direct or indirect biomarkers (33).

The dSIR and drSIR sequences might also assist with the characterization of different patterns of vascular white matter hyperintensities, and allow determination of predictive stroke recovery profiles. dSIR and drSIR sequences (especially at high field and with some form of contrast enhancement) may also allow evaluation of the glymphatic system in the various inflammatory and degenerative diseases in which abnormal CSF clearance is being increasingly recognized as a contributory factor (34).

Counter-intuitive features, sticking points, and answers to frequently asked questions

Some counter-intuitive features, sticking points and answers to frequently asked questions associated with dSIR and drSIR sequences are listed below:

(i) The graphics used to explain contrast with T_1-filters differ from the approaches conventionally used to explain T_1 contrast. Instead of a positively sloped exponential recovery for T_1 (*Figure 1*), the T_1-filter has a negative slope (*Figure 3*). Likewise, instead of an exponential decay of T_2 (*Figure 1*), the T_2-filter has a positive slope (*Figure 4*). The graphics appear contradictory unless it is recognized that the variable along the X axis is time with the conventional approach, and either T_1 or T_2 with the T_1 or T_2-filters;

(ii) The concept of nulling signals from both normal and abnormal tissues in order to increase their visibility is counterintuitive. This is then followed first by subtraction of the remaining signal, and then by division of this, and appears likely to just result in noise. It generally requires modeling of the contrast using T_1-filters approach to understand how this can be productive (*Figures 8-13*);

(iii) In general terms, increase in contrast of up to about 15 times over conventional T_1-weighted IR sequences seems improbable. This high amplification is only for small changes in T_1 in the mD, and is not across the board. However, if this amplification is correctly targeted at small changes in T_1, it may be exactly what is needed to produce high contrast from these changes;

(iv) The conventional teaching on partial volume effects between two tissues is that these result in signals intermediate between those of the two tissues. Production of high contrast boundaries from partial volume effects with signals much greater than that of either of the contributing tissues appears counterintuitive. It is useful to refer to the dSIR and drSIR T_1-bipolar filters to explain this as in *Figures 14-18*;

(v) dSIR images appear similar to highly T_2-weighted images such as T_2-wSE and T_2-FLAIR in terms of the sign of white matter gray matter contrast, and high signals from lesions, but dSIR images are highly T_1-weighted, not T_2-weighted. The use of dSIR T_1-bipolar filters explains how this is possible and the drSIR T_1-bipolar filter shows how the contrast can be reversed to produce more conventional T_1-weighted appearances of the

brain;

(vi) CSF signals in brain images are usually very low as with T_1-wSE, TI_i IR and T_2-FLAIR images, or very high as with T_2-wSE images. The dSIR and drSIR images usually show CSF as intermediate signal which does not fit either category. Again, the dSIR and drSIR T_1-bipolar filters explain how this comes about;

(vii) It is often assumed that advanced mathematics is required to understand MR contrast. The contrast behavior described in this paper can be understood using primary school arithmetic and secondary school algebra, geometry and calculus together with math teaching apps (e.g., WolframAlpha). The equations necessary for this are included in the text;

(viii) The descriptive terms used to describe TP-filters are derived from resistance inductance, capacitance (RLC) filters in electronics which have similar shapes and functional descriptions such as low pass, high pass and notch. The terms are borrowed and analogous. Their use does not imply that an electronic model is being employed to understand contrast (20);

(ix) The use of T_1 3–4 times to generate synergistic contrast with the dSIR and drSIR sequences comes from the numerator where T_1 is used twice to increase the slope of the SIR filter in the mD, and in the denominator where T_1 is used twice as an addition which can be regarded as a single or double use of T_1. The latter increases the slope of the dSIR and drSIR T_1-bipolar filters in the mD and thus the size of the T_1 contrast that is generated by changes in T_1 in the mD;

(x) T_2-wSE and T_2-FLAIR utilize changes in T_2 to produce contrast but dSIR and drSIR sequences use changes in T_1. Often there are concurrent changes in T_1 and T_2 in disease so either or both of T_1 and T_2 can be exploited to produce contrast;

(xi) In an historical context, the IR sequences necessary to produce dSIR and drSIR images have existed on clinical MR systems for at least 40 years (1). However, it is probable that the noise and artefacts present on MR systems at these earlier times would have limited the useful amplification that could have been attained had they been implemented;

(xii) The ease of implementation of dSIR and drSIR techniques which use sequences that are already on systems seems unusual for a significant advance in clinical imaging;

(xiii) The dSIR and drSIR sequences are specifically T_1-weighted rather than conventionally T_1-weighted as with SE sequences of the brain. These conventional sequences also have ρ_m-weighting and may actually be T_2-weighted when imaging the Achilles tendon (23);

(xiv) The dSIR and drSIR sequences can, in principle, be used at any static field strength but amplification may be more noise and/or artifact limited at low and ultra-low field strengths;

(xv) The principles are also applicable to other organs besides the brain.

TP-filters and CCT apps

Understanding the contrast behavior of the dSIR and drSIR sequences can be greatly facilitated by use of interactive Apps based on T_1-filters. These demonstrate contrast, allow comparisons to be made, and make it possible to simulate contrast behavior almost in real time.

Conclusions

The dSIR and drSIR sequences can produce an order of magnitude increase in contrast and be targeted at normal or near normal white matter or gray matter in a wide range of disease of the brain where subtle abnormalities in T_1 are present. A particular example is chronic neuroinflammation. This is associated with many diseases but it may be low grade and produce relatively small changes in T_1 and T_2, and therefore may not produce contrast that is apparent using conventional sequences (35).

Validation of the findings obtained with dSIR and drSIR sequences by comparison with other MRI techniques and other forms of imaging as well as histology will be necessary.

The dSIR and drSIR sequences have the potential to produce a substantial advance in clinical MRI by providing unequivocal demonstration of abnormalities that are not seen, or only poorly seen with conventional sequences. The dSIR and drSIR sequences can also produce more certainty about the absence of disease in normal appearing tissues than conventional sequences.

Acknowledgments

The authors wish to thank Dr. Nivedita Agarwal (Head

of Neuroradiology, Research Institute Eugenio Medea, Lombardy, Italy) for providing the image used in *Figure 19*. *Funding:* This study was supported by NIH (Nos. RF1AG075717, R01AR062581, R01AR068987, R01AR079484, and R21AR075851); the VA Clinical Science Research & Development Service (No. I01CX002211); GE Healthcare (Nos. A-31, A-32, and A-33) as well as from Kānoa, New Zealand and Trust Tairāwhiti, New Zealand.

Footnote

Conflicts of Interest: All authors have completed the ICMJE uniform disclosure form (available at https://qims.amegroups.com/article/view/10.21037/qims-23-232/coif). JD serves as an unpaid editorial board member of *Quantitative Imaging in Medicine and Surgery*. MNJP is a scientific and technical adviser to Magnetica, Brisbane, Australia. GMB is a clinical consultant to Magnetica, Brisbane, Australia. The other authors have no conflicts of interest to declare.

Ethical Statement: The authors are accountable for all aspects of the work in ensuring that questions related to the accuracy or integrity of any part of the work are appropriately investigated and resolved.

References

1. Young IR, Hall AS, Pallis CA, Legg NJ, Bydder GM, Steiner RE. Nuclear magnetic resonance imaging of the brain in multiple sclerosis. Lancet 1981;2:1063-6.
2. Bailes DR, Young IR, Thomas DJ, Straughan K, Bydder GM, Steiner RE. NMR imaging of the brain using spin-echo sequences. Clin Radiol 1982;33:395-414.
3. Bydder GM, Steiner RE, Young IR, Hall AS, Thomas DJ, Marshall J, Pallis CA, Legg NJ. Clinical NMR imaging of the brain: 140 cases. AJR Am J Roentgenol 1982;139:215-36.
4. Crooks LE, Mills CM, Davis PL, Brant-Zawadzki M, Hoenninger J, Arakawa M, Watts J, Kaufman L. Visualization of cerebral and vascular abnormalities by NMR imaging. The effects of imaging parameters on contrast. Radiology 1982;144:843-52.
5. Lukes SA, Crooks LE, Aminoff MJ, Kaufman L, Panitch HS, Mills C, Norman D. Nuclear magnetic resonance imaging in multiple sclerosis. Ann Neurol 1983;13:592-601.
6. Carr DH, Brown J, Bydder GM, Weinmann HJ, Speck U, Thomas DJ, Young IR. Intravenous chelated gadolinium as a contrast agent in NMR imaging of cerebral tumours. Lancet 1984;1:484-6.
7. Bydder GM, Young IR. MR imaging: clinical use of the inversion recovery sequence. J Comput Assist Tomogr 1985;9:659-75.
8. Redpath TW, Smith FW. Technical note: use of a double inversion recovery pulse sequence to image selectively grey or white brain matter. Br J Radiol 1994;67:1258-63.
9. De Coene B, Hajnal JV, Gatehouse P, Longmore DB, White SJ, Oatridge A, Pennock JM, Young IR, Bydder GM. MR of the brain using fluid-attenuated inversion recovery (FLAIR) pulse sequences. AJNR Am J Neuroradiol 1992;13:1555-64.
10. Wattjes MP, Ciccarelli O, Reich DS, Banwell B, de Stefano N, Enzinger C, et al. 2021 MAGNIMS-CMSC-NAIMS consensus recommendations on the use of MRI in patients with multiple sclerosis. Lancet Neurol 2021;20:653-70.
11. Rudà R, Capper D, Waldman AD, Pallud J, Minniti G, Kaley TJ, Bouffet E, Tabatabai G, Aronica E, Jakola AS, Pfister SM, Schiff D, Lassman AB, Solomon DA, Soffietti R, Weller M, Preusser M, Idbaih A, Wen PY, van den Bent MJ. EANO - EURACAN - SNO Guidelines on circumscribed astrocytic gliomas, glioneuronal, and neuronal tumors. Neuro Oncol 2022;24:2015-34.
12. Barkhof F, Jager HR, Thurnher M, Rovira A (Eds). Clinical Neuroradiology: the ESNR textbook. Springer International Publishing, Cham, Switzerland 2019.
13. Marques JP, Kober T, Krueger G, van der Zwaag W, Van de Moortele PF, Gruetter R. MP2RAGE, a self bias-field corrected sequence for improved segmentation and T1-mapping at high field. Neuroimage 2010;49:1271-81.
14. Spini M, Choi S, Harrison DM. 7T MPFLAIR versus MP2RAGE for Quantifying Lesion Volume in Multiple Sclerosis. J Neuroimaging 2020;30:531-6.
15. Demortière S, Lehmann P, Pelletier J, Audoin B, Callot V. Improved Cervical Cord Lesion Detection with 3D-MP2RAGE Sequence in Patients with Multiple Sclerosis. AJNR Am J Neuroradiol 2020;41:1131-4.

16. Fan S, Ma Y, Lv X, Du J, Bydder GM, Szevereny NM. Demonstration of abnormal cortical layers in Alzheimer's disease using subtracted tissue attenuated inversion recovery (STAIR) pulse sequences. Honolulu: ISMRM 2362, 2017.
17. Speckter H, Bido J, Hernandez G, Rivera D, Suazo L, Valenzuela S, Fermin R, Oviedo J, Foerster B, Gonzalez C, Stoeter P. Inversion recovery sequences improve delineation of optic pathways in the proximity of suprasellar lesions. J Radiosurg SBRT 2018;5:115-22.
18. Beaumont J, Saint-Jalmes H, Acosta O, Kober T, Tanner M, Ferré JC, Salvado O, Fripp J, Gambarota G. Multi T1-weighted contrast MRI with fluid and white matter suppression at 1.5 T. Magn Reson Imaging 2019;63:217-25.
19. Beaumont J, Gambarota G, Saint-Jalmes H, Acosta O, Ferré JC, Raniga P, Fripp J. High-resolution multi-T_1-weighted contrast and T_1 mapping with low B1>+ sensitivity using the fluid and white matter suppression (FLAWS) sequence at 7T. Magn Reson Med 2021;85:1364-78.
20. Young IR, Szeverenyi NM, Du J, Bydder GM. Pulse sequences as tissue property filters (TP-filters): a way of understanding the signal, contrast and weighting of magnetic resonance images. Quant Imaging Med Surg 2020;10:1080-120.
21. Ma YJ, Fan S, Shao H, Du J, Szeverenyi NM, Young IR, Bydder GM. Use of Multiplied, Added, Subtracted and/or FiTted Inversion Recovery (MASTIR) pulse sequences. Quant Imaging Med Surg 2020;10:1334-69.
22. Ma YJ, Shao H, Fan S, Lu X, Du J, Young IR, Bydder GM. New options for increasing the sensitivity, specificity and scope of synergistic contrast magnetic resonance imaging (scMRI) using Multiplied, Added, Subtracted and/or FiTted (MASTIR) pulse sequences. Quant Imaging Med Surg 2020;10:2030-65.
23. Ma YJ, Moazamian D, Cornfeld DM, Condron P, Holdsworth SJ, Bydder M, Du J, Bydder GM. Improving the understanding and performance of clinical MRI using tissue property filters and the central contrast theorem, MASDIR pulse sequences and synergistic contrast MRI. Quant Imaging Med Surg 2022;12:4658-90.
24. Cianfoni A, Martin MG, Du J, Hesselink JR, Imbesi SG, Bradley WG, Bydder GM. Artifact simulating subarachnoid and intraventricular hemorrhage on single-shot, fast spin-echo fluid-attenuated inversion recovery images caused by head movement: A trap for the unwary. AJNR Am J Neuroradiol 2006;27:843-9.
25. Bydder GM. The Mackenzie Davidson Memorial Lecture: detection of small changes to the brain with serial magnetic resonance imaging. Br J Radiol 1995;68:1271-95.
26. Bullock DN, Hayday EA, Grier MD, Tang W, Pestilli F, Heilbronner SR. A taxonomy of the brain's white matter: twenty-one major tracts for the 21st century. Cereb Cortex 2022;32:4524-48.
27. Planche V, Su JH, Mournet S, Saranathan M, Dousset V, Han M, Rutt BK, Tourdias T. White-matter-nulled MPRAGE at 7T reveals thalamic lesions and atrophy of specific thalamic nuclei in multiple sclerosis. Mult Scler 2020;26:987-92.
28. O'Reilly T, Webb AG. In vivo T_1 and T_2 relaxation time maps of brain tissue, skeletal muscle, and lipid measured in healthy volunteers at 50 mT. Magn Reson Med 2022;87:884-95.
29. Wei Z, Jang H, Bydder GM, Yang W, Ma YJ. Fast T_1 measurement of cortical bone using 3D UTE actual flip angle imaging and single-TR acquisition (3D UTE-AFI-STR). Magn Reson Med 2021;85:3290-8.
30. Chang L, Alicata D, Ernst T, Volkow N. Structural and metabolic brain changes in the striatum associated with methamphetamine abuse. Addiction 2007;102 Suppl 1:16-32.
31. Kolb H, Absinta M, Beck ES, Ha SK, Song Y, Norato G, Cortese I, Sati P, Nair G, Reich DS. 7T MRI Differentiates remyelinated from demyelinated multiple sclerosis lesions. Ann Neurol 2021;90:612-26.
32. Cairns J, Vavasour IM, Traboulsee A, Carruthers R, Kolind SH, Li DKB, Moore GRW, Laule C. Diffusely abnormal white matter in multiple sclerosis. J Neuroimaging 2022;32:5-16.
33. Blackmon K, Kuzniecky R, Barr WB, Snuderl M, Doyle W, Devinsky O, Thesen T. Cortical gray-white matter blurring and cognitive morbidity in focal cortical dysplasia. Cereb Cortex 2015;25:2854-62.
34. Ringstad G, Eide PK. Cerebrospinal fluid tracer efflux to parasagittal dura in humans. Nat Commun 2020;11:354.
35. Laule C, Port JD. editors. Imaging Neuroinflammation. Cambridge: Academic Press, 2023.

Cite this article as: Ma YJ, Moazamian D, Port JD, Edjlali M, Pruvo JP, Hacein-Bey L, Hoggard N, Paley MNJ, Menon DK, Bonekamp D, Pravatà E, Garwood M, Danesh-Meyer H, Condron P, Cornfeld DM, Holdsworth SJ, Du J, Bydder GM. Targeted magnetic resonance imaging (tMRI) of small changes in the T_1 and spatial properties of normal or near normal appearing white and gray matter in disease of the brain using divided subtracted inversion recovery (dSIR) and divided reverse subtracted inversion recovery (drSIR) sequences. Quant Imaging Med Surg 2023;13(10):7304-7337. doi: 10.21037/qims-23-232

